Spectrum Sharing and Energy Harvesting for IoT Networks

M.Tech. Thesis

by

Jonnalagadda Sharanya

(2002102003)

DEPARTMENT OF ELECTRICAL ENGINEERING

INDIAN INSTITUTE OF TECHNOLOGY INDORE

JUNE 2022

Spectrum Sharing and Energy Harvesting for IoT Networks

A THESIS

Submitted in partial fulfillment of the requirements for the award of the degree
of
Master of Technology

Submitted by
Jonnalagadda Sharanya

Under the supervision of
Prof. Prabhat Kumar Upadhyay

DEPARTMENT OF ELECTRICAL ENGINEERING
INDIAN INSTITUTE OF TECHNOLOGY INDORE

JUNE 2022

INDIAN INSTITUTE OF TECHNOLOGY INDORE

CANDIDATE'S DECLARATION

I hereby certify that the work which is being presented in the thesis entitled **"Spectrum Sharing and Energy Harvesting for IoT Networks"** in the partial fulfillment of the requirements for the award of the degree of **Master of Technology** and submitted in the **Department of Electrical Engineering, Indian Institute of Technology Indore**, is an authentic record of my own work carried out during the time period from June 2021 to June 2022 under the supervision of Dr. Prabhat Kumar Upadhyay, Professor, Indian Institute of Technology Indore.

The matter presented in this thesis has not been submitted by me for the award of any other degree of this or any other institute.

J. Sharanya 01-06-2022
Signature of the student
Jonnalagadda Sharanya

This is to certify that the above statement made by the candidate is correct to the best of my/our knowledge.

01-06-2022
Signature of Thesis Supervisor
Prof. Prabhat Kumar Upadhyay

Jonnalagadda Sharanya has successfully given her MTech. Oral Examination held on 06/06/2022.

Signature of Supervisor of MTech. thesis
Date: 06/06/2022

Convener, DPGC
Date: 06/06/2022

Signature of PSPC Member 1
Date: 06/06/2022
Dr. Amod C. Umarikar

Somnath Dey
Signature of PSPC Member 2
Date: 06/06/2022
Dr. Somnath Dey

ACKNOWLEDGMENT

I would like to express my sincere gratitude to my thesis supervisor **Prof. Prabhat Kumar Upadhyay**, for his constant support, encouragement and guidance during my Master's study and thesis work. Furthermore, I would like to express my deep gratitude to my PSPC members **Dr. Amod C. Umarikar** and **Dr. Somnath Dey** for their valuable suggestions and feedback.

It is their help and support, due to which I became able to complete design the technical report. Without their support this report would not have been possible.

I would also like to express my sincere gratitude and special thanks to **Mr. Alok Kumar Shukla** and **Mr. Chandan Kumar Singh** for their support in the lab work.

IIT Indore played a vital role in providing me with the facilities, teaching assistantship, lab computer and library resource that added to my knowledge and my project.

All this was made possible by incredible support and blessings of my parents who blessed me all the time, it would not have been possible without their love and support.

Jonnalagadda Sharanya
(2002102003)
M.Tech. II Year
Department of Electrical Engineering
IIT Indore

ABSTRACT

This thesis proposes a simultaneous wireless information and power transfer (SWIPT) enabled Internet of Things (IoT) based coordinated direct and relay (CDRT) transmission with non-orthogonal multiple access (NOMA) system. It incorporates overlay cognitive radio (CR) and time switching (TS)-based SWIPT technology to enhance spectrum utilization and energy efficiency. The proposed system comprises of a primary network with primary transmitter and its intended receivers (UE1, UE2), accompanied by an energy-constrained secondary transmitter, and its designated secondary receiver (IoT-U). The primary transmitter communicates directly with its strong user UE1 and exploits the secondary transmitter as an IoT-relay to communicate with a weak user UE2. The IoT-relay node employs TS-based receiver architecture and decode-and-forward protocol to convey the weak user's information along with its own information by following the NOMA principle. The same system is also studied by considering power splitting protocol to provide novelty for the considered system model and also implemented caching scheme in the proposed system model. Also, the cache pre-fetches the primary and secondary popular file contents which reduces the data access delay and increases the transmission rate.

The performance of the proposed system is evaluated in terms of outage probability, throughput and energy efficiency by considering both the perfect and imperfect successive interference cancellation at the legitimate users over Nakagami-*m* fading and in the second system model we implemented cache scheme over Rayleigh fading to provide better insights of the system model. Further, to improve the spectrum utilization we also studied the cooperation between primary and secondary networks via content caching scheme under Rayleigh fading channel. Moreover, the impact of key parameters is also highlighted, which lays the guidelines for the practical design of energy-efficient and spectrum-efficient futuristic wireless communication networks.

CONTENTS

LIST OF FIGURES

LIST OF ACRONYMS

Acronym		Definition
AWGN	-	Additive white Gaussian noise
BS	-	Base station
CDRT	-	Coordinated direct and relay transmission
CRN	-	Cognitive radio network
CSI	-	Channel state information
DF	-	Decode-and-forward
EE	-	Energy efficiency
EH	-	Energy harvesting
HD	-	Half-duplex
i.i.d	-	Independent and identically distributed
IoT	-	Internet of Things
ipSIC	-	Imperfect successive interference cancellation
IT	-	Information transmission
MIMO	-	Multiple-input multiple-output
MS	-	Mobile station
NOMA	-	Non-orthogonal multiple access
OMA	-	Orthogonal multiple access
OP	-	Outage probability
PN	-	Primary network
pSIC	-	Perfect successive interference cancellation
PT	-	Primary transmitter
PU	-	Primary user
QoS	-	Quality of service
RF	-	Radio frequency

RSI	-	Residual self-interference
SI	-	Self-interference
SIC	-	Successive interference cancellation
SINR	-	Signal-to-interference plus noise ratio
SN	-	Secondary network
SNR	-	Signal-to-noise ratio
SR	-	Secondary receiver
ST	-	Secondary transmitter
SU	-	Secondary user
SWIPT	-	Simultaneous wireless information and power transfer
TS	-	Time switching
TSC	-	Time switching cooperation
UE1	-	Primary near user
UE2	-	Primary far user
WPT	-	Wireless power transfer
ZFBF	-	Zero-forcing beamforming

Chapter 1

INTRODUCTION

In recent years, the Internet of Things (IoT) has been highlighted for its ability to connect things in the physical world with wireless applications [1], such as body area network [2], device-to-device [3], and vehicle-to-vehicle [4] communications. So IoT is a key technology by which we can able to produce various internet applications. IoT is a system that unites physical objects with virtual world. It is a intelligent technique which reduces human effort as well as easy access to physical devices. However, when large number of devices connected in a network, the spectrum usage will increase exponentially and finally results in spectrum shortage [5]. Cognitive radio (CR) and non-orthogonal multiple access (NOMA) are key technologies that address the spectrum scarcity challenge and provide massive device connectivity with higher spectrum efficiency (SE). Along with NOMA technology, one more promising technology that deals with spectrum usage is Cognitive Radio Network (CRN). In [6], it was first identified that NOMA is a special case of CRN, where the user which experiences better channel condition is named as secondary user (SU) while the user which experiences poor channel condition is named as primary user (PU). By utilizing CR technology, secondary and primary users can coexist in the same spectrum bands by effectively discarding interference and collision, improves the SE measures [7]. Out of many competitors of fifth-generation (5G) communications, NOMA is considered a promising technology that improves SE by many times. This makes NOMA a promising candidate for IoT sensor networks [8]. The principle idea of NOMA is to employ superposition coding to multiplex the multiple users' signals at the transmitter, and then to perform successive interference cancellation (SIC) at the receiver side to decode the signals in the power domain [9].

Integration of NOMA into CR, referred to as cognitive NOMA (CNOMA), has described the capability to achieve higher SE while simultaneously reducing the complexity of the power allocation (PA) design [10]. It can potentially fulfil the requirement of a 5G wireless network that provides a high throughput, broad connectivity, and low latency. Many research investigations have been coordinated around the application of CNOMA employing the underlay [11]-[12] and overlay [13]-[15] CR techniques. In [11], large-scale underlay CR networks employing the NOMA technique were investigated to improve the connectivity of secondary users (SUs). The researches revealed that the NOMA users outperformed orthogonal multiple access (OMA) users when target data rates and PA factor were carefully taken into the consideration. The outage performance of SU for underlay CNOMA network has been investigated considering decode-and-forward (DF) relaying protocol in [12]. In contrast to the underlay CNOMA, the overlay CNOMA model has been examined in [13], [14], where the secondary transmitter (ST) acts as a relay for the primary user (PU) as well as communicates with its intended secondary receivers (SRs). Moreover, authors in [17]-[21] have studied the performance of overlay CNOMA system modified for IoT environment.

Another strategy that can maximize SE of 5G wireless networks is utilizing CNOMA in coordinated direct and relay transmission (CDRT), in which a strong user is directly communicated by the source and weak user signal is transmitted from the source via half duplexing relay. Authors in [22] have studied the NOMA with CDRT and demonstrated that the proposed scheme outperforms the NOMA without CDRT in terms of ergodic sum capacity (ESC). In [23], authors investigated device-to-device aided NOMA-based CDRT network where the proposed network outperforms the conventional CDRT network in terms of ESC and sum throughput. Very recently, by considering IoT-based CDRT with NOMA assisted network, the system performance was examined for the outage probability (OP) and ESC [24]. Authors in [25] examined the OP performance of a satellite assisted CDRT-NOMA system. In [26], the OP performance of near and far user was investigated in CNOMA-based CDRT system, where an energy harvesting method was introduced to assist base station signal transmission to the far user. In [27], an efficient and best relay selection was proposed for a multi relay systems to achieve successful decoding at strong users.

Besides SE improvement of IoT-based CNOMA-CDRT network, energy efficiency (EE) is another key parameter that should be considered while designing a futuristic 5G wireless network to enhance the lifespan. Recent studies indicate that the power requirement of IoT sensors and devices could be met by harvesting energy from radio frequency (RF) signals. In fact, RF signals carry information and energy both. The IoT sensors or nodes can recharge themselves by harvested energy from RF signals while simultaneously decoding the information data and relaying or transmitting the source node's information to its destination [24]. Among the potential energy harvesting (EH) techniques, simultaneous wireless information and power transfer (SWIPT) has received much attention as the key enabling technique for future IoT networks [28]. Two practical receiver architectures have been investigated to expedite SWIPT in wireless networks, namely time-switching (TS) and power-splitting (PS) [29]. In TS-based receiver architecture, the receiver alternates between the EH mode and the information decoding mode over the course of the transmission. Unlike TS, PS-based receiver architecture splits the received signal power between EH and information transmission. Authors in [30] studied an IoT-based system set up to examine the outage performance of a cooperative NOMA network where the energy-constrained IoT primary node acts as PS-based EH-relay, which conveys the source's information and its own information following the NOMA principle. In [31], the outage performance of near and far users was investigated for the SWIPT assisted cooperative NOMA-CDRT system and compared with the conventional OMA system.

The research mentioned above mainly investigated the impact of deploying NOMA in CR networks [11]-[14] while EH has received less attention in the context of IoT implementations. The research work in [17]-[21] emphasized the NOMA based CDRT network but have considered the ideal case of perfect SIC (pSIC) and analysed the system performance over Rayleigh fading channel. However, it is challenging to implement the pSIC in a practical scenario considering error propagation and complexity scaling [28]. Also, it is clear from the literature survey that employing EH with CNOMA-CDRT network is still unexplored. Inspired by these studies, we propose a SWIPT enabled IoT based CNOMA-CDRT system considering both pSIC and imperfect SIC (ipSIC). The IoT-relay employs TS-based receiver architecture for EH, and operates in a DF relaying mode.

Wireless caching is an important technique used in present and future wireless networks. Caching at the wireless edge is a unique way of boosting spectral efficiency and reduces energy consumption of wireless systems. The performance of cache-aided SWIPT NOMA - CDRT systems, in which source or base station communicates with far users by the use of relay. To increase the relay serving time, the relay is assumed to be incorporated with a caching and a EH capability. On the basis of power-splitting mechanism, the effect of caching on the system performance measures analysed in terms of the system throughput and the energy efficiency.

Authors in [29] studied the various technologies that can be incorporated along with NOMA which can give us brief insights of caching that is implemented with NOMA. In [30], authors proposed a new approach to wireless caching for scenarios in which the cache content has to be updated during on-peak hours. In [31], authors have investigated the content caching along with primary and secondary cooperation scheme to improve the spectrum utilization. In [32], authors considered caching scheme at the IoT gateway, in which IoT information is stored and directly sent to the users that helps in reducing the data traffic in IoT network as well as energy consumed by IoT sensor nodes. In [33], authors focused on cache and EH enabled D2D cellular network in which mobile user can fetch the cache contents from core content server or base station and it can be charged by using EH capability. Along with this they also focused on energy states and requested contents along with content caching and also they have considered three modes self-satisfied, D2D communication and cellular downlink communication in which each mobile user can fetch its requested file contents. Authors in [34], have incorporated the caching capabilities into SWIPT system and tried to improve the serving time, throughput and energy harvesting performance at the relays.

Key Contributions:

In summary, the key contributions of this article are emphasized as follows:

We propose a SWIPT enabled IoT-based CNOMA-CDRT network in which cellular primary network collaborates with a cognitive IoT network to further improve primary far user performance by exploiting the NOMA principle. In view of the practical implementation of the proposed work, we investigate the impact of pSIC and ipSIC on the performance of the proposed system.

- For the proposed system model, we analysed the outage performance of both primary and secondary networks under the pSIC/ipSIC cases. For this, we analytically derive the expressions of the OP for pSIC/ipSIC cases based on their received signal-to-noise ratios

(SNRs) and signal-to-interference-plus-noise ratios (SINRs) over Nakagami-*m* fading environment.

- With the derived OP expressions, we evaluate the system throughput and EE to gain further insights into the considered system.

The second contribution of this work is we propose a cache-assisted SWIPT system in which we study the interaction between SWIPT and content caching. First, in terms of the content caching and transmission strategies, we provide a cooperation scheme to maximize secondary users effective data transmission rates under the constraint of the primary users target rate under Rayleigh fading channel consideration.

Organization of the Thesis:

The remaining part of the thesis is organized as follows.

- Chapter 2 presents SWIPT enabled IoT based CDRT-NOMA system. In this we calculate OP for each user and try to maximize system throughput to improve SE and also we focus on EE of the proposed system.
- Chapter 3 presents cache aided SWIPT with EH relay. Here, we study the interaction between caching capacity and SWIPT in the considered system.
- Chapter 4 presents the conclusion and future scope of the work presented in this thesis.

Chapter 2

SWIPT Enabled IoT-based Coordinated Direct and Relay Transmission with Non-Orthogonal Multiple Access

2.1. Introduction:

One of the most promising techniques of fifth generation communication that has drawn significant attention in present is Non-orthogonal multiple access (NOMA) which has shown great impact in boosting the spectral efficiency (SE). By exploiting NOMA technique, multiple users can be served by a single source with distinct power levels which helps to improve spectral efficiency. In addition to this energy efficiency (EE) is considered as one of the important performance measure of wireless networks and this can be improved by collecting energy from ambient environments, because information and energy can be jointly conveyed by radio-frequency signals. Along with this, simultaneous wireless information and power transfer (SWIPT) is served as an effective solution to improve the EE performance by overcoming the challenges that are resulted from the increasing power consumption.

2.2. System Model:

2.2.1 Description:

Here, we propose an SWIPT enabled IoT-based CDRT system with overlay CNOMA for a single cluster as shown in Fig. 2.1. This system consists of two networks namely, primary network (PN) and a secondary network (SN). Here, PN includes a primary transmitter node PT also known as primary base station, primary near user UE1, and a primary far user UE2, whereas the SN consists of a energy constrained IoT-relay ST and IoT user (IoT-U). In this system model, we assumed that direct link is present between PT and UE1, whereas absence of direct link between PT and UE2 due to poor channel conditions between them. Throughout this thesis, subscripts notations p,s,1,2,r are used to represent PT,ST,UE1,UE2 and IoT-U respectively.

It is clear from above mentioned points that, as there is no direct communication between PT and far users, some assisting nodes like relaying nodes are required in between them to make communication possible. Hence, instead of using multiple relay nodes, ST has an radio frequency based EH capability and acts a dedicated decode–and-forward (DF) relay node between PT and far user to assist primary communication. In exchange of cooperation, relay is able to simultaneously transmit its own signal to its IoT-U by exploiting NOMA. Also, all the sensors are equipped with a single antenna due to their limited size and operate in half-duplex mode. The channel gain between any two nodes i and j is represented as $|h_{i,j}|^2$ where $i \in$ (p.s) and $j \in$ (1,2,s,r) with $i \neq j$ and experience Nakagami-m fading plus additive white Gaussian noise with zero mean and noise variance σ^2 i.e.$CN(0, \sigma^2)$.

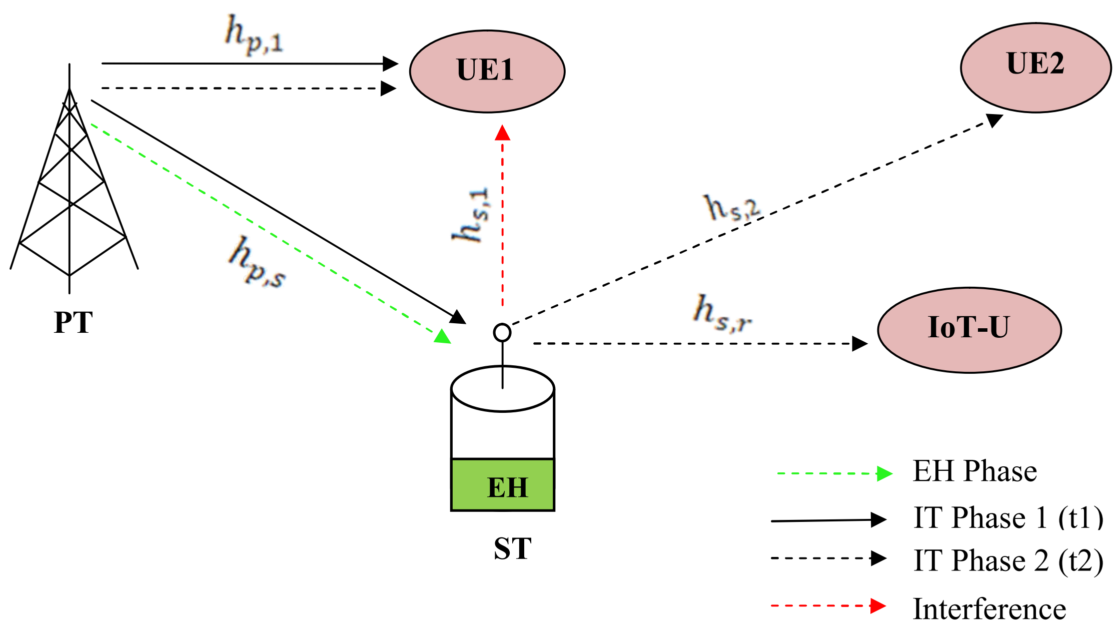

Fig. 2.1: Proposed SWIPT based NOMA CDRT system for a single cluster

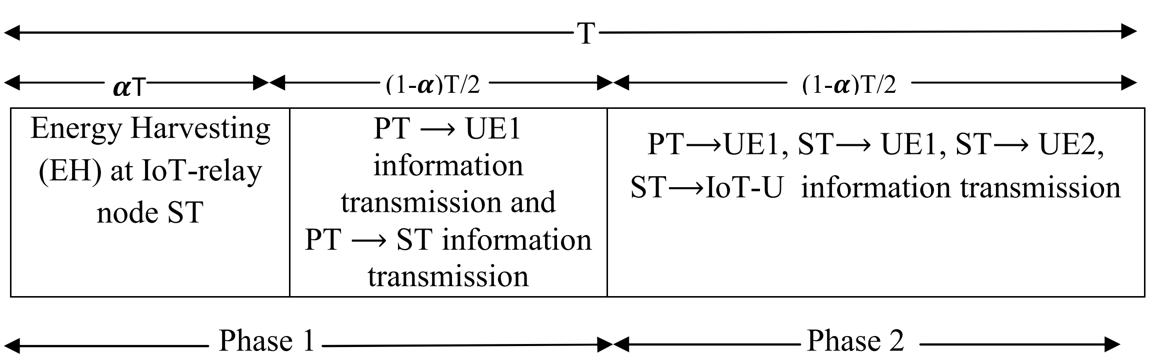

Fig. 2.2: Time switching protocol for EH and IT phases

TSC protocol is implemented in this system for energy harvesting (EH) and information transmission (IT) as shown in Fig. 2.2. In the TSC protocol, the transmission block time T is divided into three sub-blocks with α ∈ (0, 1) denoting the TSC parameter. The duration αT represents the EH time that IoT-relay takes to harvest energy from PT and the remaining time $(1 - \alpha)T$ is used for IT. Given the half-duplex operation, the time $(1-\alpha)T/2$ is dedicated for ST, ST to receive information from PT, and the remainder $(1 - \alpha)T/2$ is used for IT from ST to UE1, UE2, and SR and during this phase UE1 also receive information from PT.

2.2.2. Energy Harvesting (EH) Phase:

The harvested energy at ST during αT is given by

$$E_h = \eta P_P |h_{p,s}|^2 \alpha T, \tag{2.1}$$

where $\eta \in (0,1)$ is the energy conversion efficiency it depends on the rectification process and the EH circuitry and P_P is the source transmit power. Hence, the transmit power of node S over the time $(1 - \alpha)T/2$ can be obtained as

$$P_s = \frac{E_h}{(1-\alpha)T/2} = \frac{2\alpha\eta P_P |h_{p,s}|^2}{1-\alpha}. \tag{2.2}$$

2.2.3. Information Transmission (IT) Phase:

In the proposed system model overall information transmission takes place in two phases and each phase requires one time slot. In both the phases NOMA transmission technique is being employed. IT Phase 1 is denoted as t1, and IT Phase 2 denoted as t2.

During t1 phase, P transmits its composite signal $X_p = \sqrt{\psi_1 P_p} x_1 + \sqrt{\psi_2 P_p} x_2$ to nodes ST and UE1 using downlink NOMA transmission principle. Here, ψ_1 and x_1 are power allocation factor and data symbol related to UE1 whereas ψ_2 and x_2 are the power allocation factor and data symbol related to UE2 respectively and assuming x_2 as high powered symbol compared to x_1 thus, we can write $\psi_2 > \psi_1$ and $\psi_1 + \psi_2 = 1$. Thus, the received signals at node j, j ∈ (1,s) can be given as

$$y_{pj} = h_{p,j} X_p + n_{p,j}, \tag{2.3}$$

where $n_{p,j}$ is the AWGN variable. Following the NOMA principle, UE1 performs SIC to decode the x_1 symbol. Firstly, UE1 decodes x_2 symbol assuming x_1 as noise and then, after performing SIC, x_1 symbol is decoded at UE1. Thus, the SINR received at UE1 to decode x_2 can be expressed as

$$\gamma_{x_2 \rightarrow p,1}^{t_1} = \frac{\psi_2 \, \eta_p |h_{p,1}|^2}{\psi_1 \eta_p |h_{p,1}|^2 + 1}, \tag{2.4}$$

and UE1 to decode x_1 can be given as

$$\gamma_{p,1}^{t_1} = \frac{\psi_1 \eta_p |h_{p,1}|^2}{\lambda \, \psi_2 \eta_p |\hat{h}_{p,1}|^2 + 1}, \tag{2.5}$$

where $\eta_p = \frac{P_P}{\sigma^2}$ is the transmit SNR at source node and $\boldsymbol{\lambda}$ $(0 < \boldsymbol{\lambda} < 1)$ is the residual interference parameter when $\boldsymbol{\lambda}$=0 it represents pSIC. Here, $|\hat{h}_{p,1}|^2$ is the channel coefficient of residual interference signal at UE1 that experiences Nakagami-m fading with m_{p11} as fading severity parameter and Ω_{p11} as average channel power gain.

Moreover, IoT- relay will decode x_2 symbol by assuming x_1 as noise since it is a low powered symbol. Thus, the received SINR at IoT- relay node is given by

$$\gamma_{p,s}^{t_1} = \frac{\psi_2 \eta_p |h_{p,s}|^2}{\psi_1 \eta_p |h_{p,s}|^2 + 1}. \tag{2.6}$$

In the next IT phase 2 (t2), if ST is able to decode symbol x_2 at t1 then only secondary transmission will take place, otherwise ST will remain silent and no transmission takes place during this phase.

Following successful decoding of x_2 at node ST, it combines x_2 with its own signal x_r to create a superimposed signal $X_s = \sqrt{\psi_2 P_s} x_2 + \sqrt{\psi_r P_s} x_r$ by using NOMA principle, where ψ_2 and x_2 are power allocation coefficient and data symbol related to UE2 whereas ψ_r and x_r are the power allocation coefficient and data symbol related to IoT-U respectively and assuming x_2 as high powered symbol compared to x_r thus, we can write $\psi_2 > \psi_r$ and $\psi_2 + \psi_r = 1$. Thus, the received signal at UE2 and IoT-U can be given as

$$y_{s,j}^{t_2} = h_{s,j}X_s + n_{s,j}\ , \tag{2.7}$$

where $n_{s,j}$ is the AWGN variable and $j \in$ (2,r). Here, x_2 can be directly decoded at UE2 because of high power allocation, whereas SIC is employed to decode x_r at IoT-U. It first decodes x_2 considering x_r as noise and then decodes x_r by discarding x_2 using SIC. Therefore, the received SINR at UE2 to decode x_2 can be given as

$$\gamma_{s,2}^{t_2} = \frac{\psi_2 \eta_s |h_{s,2}|^2}{\psi_r \eta_s |h_{s,2}|^2 + 1}, \tag{2.8}$$

For the secondary network, the SINR received at SR to decode $\boldsymbol{x_2}$ before decoding $\boldsymbol{x_r}$ is given by

$$\gamma_{x_2 \to s.r}^{t_2} = \frac{\psi_2 \eta_s |h_{s,r}|^2}{\psi_r \eta_s |h_{s,r}|^2 + 1}, \tag{2.9}$$

The received SINR at IoT-U to decode x_r after SIC can be given as

$$\gamma_{s,r}^{t_2} = \frac{\psi_r \eta_s |h_{s,r}|^2}{\lambda\, \psi_2 \eta_s |h_r|^2 + 1}, \tag{2.10}$$

Here, $|h_r|^2$ is the channel coefficient of residual interference signal at IoT-U that experiences Nakagami - m fading with m_r as fading severity parameter and Ω_r as average channel power gain.

In order to maximize spectral utilization and the wireless channel, source node PT transmits the new signal $\widehat{x}_1$ to UE1 with transmit power $\sqrt{\psi_1^{t_2} P_p}$, $\psi_1^{t_2} \in$ (0, 1). However, during t2, UE1 faces the interference from IoT-relay node ST, which can be estimated and eliminated by using the side information of x_2 that is obtained through SIC process during t1.

Therefore, the signal received at UE1 during t2 and corresponding SINR is given, respectively, by

$$y_{(p,s),1}^{t_2} = \sqrt{\psi_1^{t_2} P_p} h_{p,1} \hat{x}_1 + h_{s,1} X_s + n_{p,1}, \tag{2.11}$$

$$\gamma_{p,1}^{t_2} = \frac{\psi_1^{t2}\eta_p|h_{p,1}|^2}{\psi_r\eta_s|h_{s,1}|^2+1}, \tag{2.12}$$

2.3. Performance Analysis:

In this section, the performance of primary and secondary networks is evaluated in terms of their OP, system-throughput, and EE by deriving analytical expressions over Nakagami-*m* fading channel. Here, we consider R_1, R_2 and R_r as predefined target rate thresholds for UE1, UE2 and IoT-U respectively.

2.3.1. Outage Probability of Primary Network:

2.3.1.1. Outage Probability of UE1:

During t1 phase, the outage event of primary user1 occurs when UE1 unable to decode both symbols x_1 and x_2, and this is given as

$$P_{out,(1,p)}^{t_1,ipSIC} = 1 - P_r\left(\gamma_{x_2\to p,1}^{t_1} > R_2^{th}\ ;\ \gamma_{p,1}^{t_1} > R_1^{th}\right). \tag{2.13}$$

where $R_1^{th} = 2^{\frac{2\,\eta\,R_1}{1-\alpha}} - 1\,, R_2^{th} = 2^{\frac{2\,\eta\,R_2}{1-\alpha}} - 1$

Now, we evaluate above Eq. (2.13) in both ipSIC and pSIC cases considering $R_2^{th} < \frac{\varphi_2}{\varphi_1}$ into account in the following sections.

a) ipSIC: $P_{out,(1,p)}^{t_1,ipSIC}$ for the ipSIC case can be evaluated through following theorem.

Theorem 1: The exact form expression of $P_{out,(1,p)}^{t_1,ipSIC}$ for ipSIC case calculated over Nakagami-*m* fading can be expressed as

$$P_{out,(1,p)}^{t_1,ipSIC} = 1 - Z_0 - Z_1, \tag{2.14}$$

the final equations for Z_0 and Z_1 are given by

$$Z_0 = \frac{\left(\frac{m_{p11}}{\Omega_{p11}}\right)^{m_{p11}}}{\Gamma(m_{p11})} \sum_{k=0}^{m_{p1}-1} \frac{\left(u_3\frac{m_{p1}}{\Omega_{p1}}\right)^k}{k!} \sum_{k_1=0}^{k} \binom{k}{k_1} (\varphi_2\eta_p)^{k_1} \sum_{k_2=0}^{m_{p11}+k_1-1} \frac{U^{k_2}(m_{p11}+k_1-1)!}{(k_2)!\,B^{m_{p11}+k_1-k_2}\, exp^{-\left(\frac{m_{p1}u_3}{\Omega_{p1}}+BU\right)}}, \tag{2.15}$$

$$Z_1 = \left(exp^{-\left(\frac{m_{p1}}{\Omega_{p1}}\right)u_2} \sum_{k=0}^{m_{p1}-1} \frac{\left(\frac{m_{p1}u_2}{\Omega_{p1}}\right)^k}{k!} \right) \left[1 - exp^{-\left(\frac{m_{p11}}{\Omega_{p11}}\right)U} \sum_{k_1=0}^{m_{p11}-1} \frac{\left(\frac{m_{p11}U}{\Omega_{p11}}\right)^{k_1}}{k_1!} \right]. \tag{2.16}$$

$$\text{where} \quad U = \frac{\frac{u_2}{u_3}-1}{\eta_p \varphi_2}, B = \frac{m_{p11}}{\Omega_{p11}} + \frac{m_{p1}u_3\eta_p\varphi_2}{\Omega_{p1}}$$

By substituting Eq. (2.15) and Eq. (2.16) in Eq. (2.14), one can get required expression for $P_{out,(1,p)}^{t_1,ipSIC}$.

Proof: Refer Appendix A.

b) pSIC: Invoking respective SINRs into Eq. (2.13) and considering $\boldsymbol{\lambda}$=0 for pSIC case, we can evaluate Eq. 2.13 as shown below.

$$= 1 - P_r\left(|h_{p,1}|^2 > \frac{R_1^{th}}{\varphi_1\eta_p}; |h_{p,1}|^2 > \frac{R_2^{th}}{(\varphi_2 - \varphi_1 R_2^{th})\eta_p} \right). \tag{2.17}$$

considering $z = |h_{p,1}|^2, u_1 = \frac{R_1^{th}}{\varphi_1\eta_p}, u_2 = \frac{R_2^{th}}{(\varphi_2-\varphi_1 R_2^{th})\eta_p}$, now above Eq. (2.17) can be modified as

$$P_{out,(1,p)}^{t_1,pSIC} = 1 - P_r(z > max\ (u_1, u_2)), \tag{2.18}$$

Case i: if $u_1 > u_2$,

$$P_r(z > u_1) = exp^{-\left(\frac{m_{p1}}{\Omega_{p1}}\right)\left(\frac{R_1^{th}}{\varphi_1\eta_p}\right)} \sum_{k=0}^{m_{p1}-1} \frac{\left(\frac{m_{p1}}{\Omega_{p1}} \frac{R_1^{th}}{\varphi_1\eta_p}\right)^k}{k!}, \tag{2.19}$$

Case ii: if $u_1 < u_2$

$$P_r(z > u_2) = exp^{-\left(\frac{m_{p1}}{\Omega_{p1}}\right)(u_2)} \sum_{k=0}^{m_{p1}-1} \frac{\left(\frac{m_{p1}}{\Omega_{p1}} u_2\right)^k}{k!}. \tag{2.20}$$

By substituting Eq. (2.19), Eq. (2.20) in above Eq. (2.18) one can get $P_{out,(1,p)}^{t_1,pSIC}$ for pSIC case.

2.3.1.2. Outage Probability of UE1 in T2 Phase:

During T2 phase in successful decoding at relay case UE1 will receive signals from both primary transmitter and relay node, then its outage event can be expressed as

$$P_{out,UE1}^{t_2} = 1 - P_r\left(\gamma_{x_2 \to p,1}^{t_1} > R_2^{th}\ ;\ \gamma_{p,1}^{t_2} > R_1^{th}\right). \tag{2.21}$$

and it can be calculated in following lemma.

Lemma 1: The exact expression of $P_{out,UE1}^{t_2}$ computed over Nakagami-m fading can be expressed as

$$P_{out,UE1}^{t_2} = 1 - Z_2 - Z_3, \tag{2.22}$$

where Z_2 and Z_3 can be given as

$$Z_2 = \sum_{k=0}^{m_{p1}-1} \frac{\left(\frac{m_{p1}u_2}{\Omega_{p1}}\right)^k}{k!} exp^{-\left(\frac{m_{p1}}{\Omega_{p1}}\right)u_2} \left(1 - \sum_{k_2=0}^{m_{s1}-1} \frac{\left(\frac{m_{s1}u_9}{\Omega_{s1}}\right)^{k_2}}{k_2!} \times 2\left(\frac{m_{s1}\Omega_{ps}}{m_{ps}\Omega_{s1}}\right)^{\left(\frac{m_{ps}-k_2}{2}\right)} \times K_{m_{ps}-k_2}\left(2\sqrt{\frac{m_{ps}m_{s1}}{\Omega_{ps}\Omega_{s1}}u_2}\right)\right) \tag{2.23}$$

$$Z_3 = \frac{2}{\Gamma(m_{s1})}\left(\frac{m_{s1}}{\Omega_{s1}}\right)^{m_{s1}} \sum_{k=0}^{m_{ps}-1} \frac{1}{k!}\left(\frac{m_{ps}\overline{u_0}}{\Omega_{ps}}\right)^k \left(\frac{m_{ps}\Omega_{s1}\overline{u_2}}{m_{s1}\Omega_{ps}}\right)^{\frac{m_{s1}-k}{2}} K_{m_{s1}-k_1}\left(2\sqrt{\frac{m_{ps}m_{s1}}{\Omega_{ps}\Omega_{s1}}u_2}\right)$$
$$- \sum_{k=0}^{m_{ps}-1} \sum_{k_1=0}^{k} \sum_{k_2=0}^{m_{p1}+k-1} \sum_{l=0}^{m_{ps}+m_{p1}-j-1} \binom{k}{k_1}\binom{m_{ps}+m_{p1}-j-1}{l}\left(\frac{m_{ps}\Omega_{s1}}{m_{s1}\Omega_{ps}\hat{u}_{11}}\right)^{k+l}\left(\frac{m_{p1}}{\Omega_{p1}}\right)^{j+l-k}$$
$$\times \frac{(-\hat{u}_1)^{k-k_1}(\hat{u}_{11})^k(-1)^l}{\Gamma(m_{p1})\Gamma(m_{s1})k!\,j!} \frac{\Gamma(m_{p1}+k_1)}{exp^{\left(\phi - \frac{m_{ps}\hat{u}_1}{\Omega_{ps}}\right)}} \Gamma(m_{s1}-k-l,\phi) \tag{2.24}$$

with $\phi = \frac{m_{ps}m_{s1}\Omega_{p1}}{\Omega_{ps}\Omega_{s1}m_{p1}\hat{u}_{11}}$. Moreover, $P_{out,UE}^{t_2}$ becomes unity for $R_2^{th} \geq \frac{\varphi_2}{\varphi_1}$.

Proof: Refer Appendix B.

2.3.1.3. Outage Probability of UE2 in IT Phase t2:

The outage event of the UE2 occurs either UE2 cannot decode its symbol x_2 or the relay node is unsuccessful in decoding. For a predefined target rate R_2 the OP of UE2 is given as below.

$$P_{out,UE2}^{t_2} = \underbrace{P_r\left(\gamma_{p,s}^{t_1} > R_2^{th}\ ;\ \gamma_{s,2}^{t_2} > R_2^{th}\right)}_{P_1} + \underbrace{P_r\left(\gamma_{p,s}^{t_1} < R_2^{th}\right)}_{P_2}. \tag{2.25}$$

By invoking respective SINR model equations into above and performing some mathematical computations on those will result in expressions given in following lemma.

Lemma 2: The analytical expression for $P_{out,UE2}^{t_2}$ over Nakagami-m fading channel conditioned on $R_2^{th} < \frac{\varphi_2}{\varphi_1}$ can be given as $P_{out,UE2}^{t_2} = P_1 + P_2$ where P_1 and P_2 computed as follows.

$$P_1 = exp^{-\left(\frac{m_{ps}}{\Omega_{ps}}u_2\right)} \sum_{k=0}^{m_{ps}-1} \frac{\left(\frac{m_{ps}u_2}{\Omega_{ps}}\right)^k}{k!} - \frac{\left(\frac{m_{s2}}{\Omega_{s2}}\right)^{m_{s2}}}{\Gamma(m_{s2})} \sum_{k=0}^{m_{s2}-1} \frac{\left(\frac{m_{s2}u_5}{\Omega_{s2}}\right)^k}{k!} \times \sum_{u=0}^{\infty} \frac{(-1)^u(\theta)^u}{u!}\, exp^{-(\theta_1 u_2)} \sum_{k_1=0}^{m_{ps}-k-u-1} \frac{\left(m_{ps}-k-u-1\right)!\,(u_2)^{k_1}}{k_1!\,(\theta_1)^{m_{ps}-k-k_1-u-1}}, \tag{2.26}$$

$$P_2 = 1 - exp^{-\left(\frac{m_{ps}}{\Omega_{ps}}u_2\right)} \sum_{k=0}^{m_{ps}-1} \frac{\left(\frac{m_{ps}u_2}{\Omega_{ps}}\right)^k}{k!}. \tag{2.27}$$

where $u_5 = \frac{R_2^{th}}{(\varphi_2-\varphi_1 R_2^{th})\,\beta\,\eta_p}$, $\theta = \frac{m_{s2}u_5}{\Omega_{s2}}$, $\theta_1 = \frac{m_{ps}}{\Omega_{ps}}$

Proof: Refer Appendix C.

2.3.2. Outage Probability of Secondary Network:

Secondary transmission takes place only when ST able to decode x_2 symbol, else secondary network will be in outage. For the IoT-U, the outage event occurs either when ST node could not detect symbol x_2 or when IoT- relay node ST unable to detect x_r along with successful detection of x_2.

For a given predefined target rate threshold R_r , the OP of secondary network can be given as

$$P_{out,sr}^{t_2} = \underbrace{P_r\left(\gamma_{p,s}^{t_1} > R_2^{th} \; ; \; \bar{P}_{sr}\right)}_{P_{out1}} + \underbrace{P_r\left(\gamma_{p,s}^{t_1} < R_2^{th}\right)}_{P_{out2}}. \tag{2.28}$$

where $R_r^{th} = 2^{\frac{2\,\eta\, R_r}{1-\alpha}}$, $\bar{P}_{sr}$ denotes the OP of IoT-U fails to detect any symbol can be given as

$$\bar{P}_{sr} = 1 - P_r\left(\gamma_{x_2\rightarrow s.r}^{t_2} > R_2^{th} \; ; \; \gamma_{s,r}^{t_2} > R_r^{th}\right), \tag{2.29}$$

After plugging respective SINRs into Eq.(2.29) and performing some algebraic manipulations, further it can be expressed as follows for ipSIC and pSIC cases, respectively.

$$\bar{P}_{sr} = P_r\left(|h_{s,r}|^2 < min\left(\frac{u_a}{|h_{p,s}|^2}, \frac{u_b\left(\varphi_2 \beta \eta_p |h_r|^2 + 1\right)}{|h_{p,s}|^2} \right)\right), \tag{2.30}$$

further, we compute $P_{out,sr}^{t_2}$ for ipSIC and pSIC cases by substituting Eq. (2.30) in Eq. (2.28) which are conditioned on $R_2^{th} < \frac{\varphi_2}{\varphi_1}$ and $R_r^{th} < \frac{\varphi_r}{\lambda\, \varphi_2}$ in subsequent sections results in

$$\begin{aligned} P_{out,sr}^{t_2,ipSIC} = & \underbrace{P_r\left(\gamma_{p,s}^{t_1} > R_2^{th} \; ; \; |h_{s,r}|^2 < \frac{u_a}{|h_{p,s}|^2} \; ; \; \frac{u_a}{|h_{p,s}|^2} > \frac{u_b\left(\varphi_2 \beta \eta_p |h_r|^2 + 1\right)}{|h_{p,s}|^2} \right)}_{P_{out,c1}} \\ & + \underbrace{P_r\left(\gamma_{p,s}^{t_1} > R_2^{th} \; ; \; |h_{s,r}|^2 < \frac{u_b\left(\varphi_2 \beta \eta_p |h_r|^2 + 1\right)}{|h_{p,s}|^2} \; ; \; \frac{u_a}{|h_{p,s}|^2} < \frac{u_b\left(\varphi_2 \beta \eta_p |h_r|^2 + 1\right)}{|h_{p,s}|^2} \right)}_{P_{out,c2}} \\ & + P_{out2} \end{aligned} \tag{2.31}$$

Proof: Refer Appendix D.

Final expressions for $P_{out,c1}, P_{out,c2}, P_{out2}$ are as follows

$$P_{out,c1} = \sum_{k=0}^{m_{ps}-1} \frac{\left(\frac{m_{ps}\phi_1}{\Omega_{ps}}\right)^k}{k!} exp^{-(\theta_1\phi_1)} - \frac{\left(\frac{m_{ps}}{\Omega_{ps}}\right)^{m_{ps}}}{\Gamma(m_{ps})} \sum_{l=0}^{m_s-1} \frac{\left(\frac{m_s u_a}{\Omega_s}\right)^l}{l!} exp^{-(\theta_1\phi_1)}$$

$$\times \sum_{u=0}^{\infty} \frac{(-1)^u(\xi_5)^u}{u!} \sum_{l_2=0}^{m_{ps}-u-l-1} \frac{(m_{ps}-u-l-1)!\,(\phi_1)^{l_2}}{l_2!\,(\theta_1)^{(m_{ps}-u-l-l_2)}}$$

$$- \left(\sum_{u=0}^{\infty} \frac{(-1)^u(\xi_3)^u}{u!} \sum_{l_3=0}^{m_{ps}-u-k-1} \frac{(m_{ps}-u-l-1)!\,(\phi_1)^{l_3}}{l_3!\,(\theta_1)^{(m_{ps}-u-k-l_3)}} - \sum_{k_1=0}^{m_s-1} \frac{\left(\frac{m_s u_a}{\Omega_s}\right)^{k_1}}{k_1!} \times \sum_{u=0}^{\infty} \frac{(-1)^u(\xi_4)^u}{u!} \sum_{l_4=0}^{m_{ps}-u-k-k_1-1} \frac{(m_{ps}-u-k-k_1-1)!\,(\phi_1)^{l_4}}{l_4!\,(\theta_1)^{(m_{ps}-u-k-k_1-l_4)}} \right)$$

$$\times \frac{\left(\frac{m_{ps}}{\Omega_{ps}}\right)^{m_{ps}}}{\Gamma(m_{ps})} \sum_{k=0}^{m_r-1} \frac{\left(\frac{m_r\phi_2}{\Omega_r}\right)^k}{k!} exp^{-(\theta_1\phi_1)}, \tag{2.32}$$

$$P_{out,c2} = \frac{\left(\frac{m_{ps}}{\Omega_{ps}}\right)^{m_{ps}}}{\Gamma(m_{ps})} \sum_{k=0}^{m_r-1} \frac{\left(\frac{m_r\phi_2}{\Omega_r}\right)^k}{k!} \sum_{u=0}^{\infty} \frac{(-1)^u(\xi_1)^u}{u!} \sum_{k_3=0}^{m_{ps}-k_2-u-1} \frac{(m_{ps}-k_2-u-1)!\,(\phi_1)^{k_3}}{(k_3)!\,(\theta_1)^{m_{ps}-u-k_2-k_3}} exp^{-(\theta_1\phi_1)}$$

$$\times \frac{\left(\frac{m_{ps}}{\Omega_{ps}}\right)^{m_{ps}}}{\Gamma(m_{ps})} \frac{\left(\frac{m_r}{\Omega_r}\right)^{m_r}}{\Gamma(m_r)} \sum_{k=0}^{m_s-1} \frac{\left(\frac{m_s}{\Omega_s}\right)^k}{k!} \sum_{k_4=0}^{k} \binom{k}{k_4} \left(u_b\varphi_2\beta\eta_p\right)^{k_4} (u_b)^{k-k_4}\, exp^{-(\theta_1\phi_1)}$$

$$\times \sum_{k_5=0}^{m_r+k_4-1} \frac{(m_r+k_4-1)!\,(\phi_2)^{k_5}}{k_5!\,(\theta_1)^{(m_r+k_4-k_5)}} \sum_{u=0}^{\infty} \frac{(-1)^u(\xi_2)^u}{u!} \sum_{k_6=0}^{m_{ps}-k+k_4-k_5-u-1} \frac{(m_{ps}+k_4-u-k-k_5-1)!\,(\phi_1)^{k_6}}{(k_6)!\,(\theta_1)^{m_{ps}-u-k+k_4-k_5-k_6}}, \tag{2.33}$$

$$P_{out2} = 1 - \sum_{k=0}^{m_{ps}-1} \frac{\left(\frac{m_{ps}\phi_1}{\Omega_{ps}}\right)^k}{k!} exp^{-(\theta_1\phi_1)}. \tag{2.34}$$

pSIC: For pSIC case with $\lambda = 0$, proceeding further gives following results.

$$\gamma_{s,r}^{t_2} = \varphi_r \eta_s |h_s|^2. \tag{2.35}$$

Therefore, $P_{out,sr}^{t_2,\,pSIC} = P_{out,c1}^{pSIC} + P_{out,c2}^{pSIC} + P_{out2}$

$$P_{out,c1}^{pSIC} = \sum_{k=0}^{m_{ps}-1} \frac{\left(\frac{m_{ps}\phi_1}{\Omega_{ps}}\right)^k}{k!} exp^{-(\theta_1\phi_1)} - \frac{\left(\frac{m_{ps}}{\Omega_{ps}}\right)^{m_{ps}}}{\Gamma(m_{ps})} \sum_{l=0}^{m_s-1} \frac{\left(\frac{m_s u_a}{\Omega_s}\right)^l}{l!} exp^{-(\theta_1\phi_1)}$$
$$\times \sum_{u=0}^{\infty} \frac{(-1)^u(\xi_6)^u}{u!} \sum_{l_2=0}^{m_{ps}-u-l-1} \frac{(m_{ps}-u-l-1)!\,(\phi_1)^{l_2}}{l_2!\,(\theta_1)^{(m_r+k_4-k_5)}}, \tag{2.36}$$

By replacing u_a with u_c and ξ_6 with ξ_7, one can get $P_{out,c2}^{pSIC}$.

where $u_a = \frac{R_2^{th}}{(\varphi_2 - \varphi_r R_2^{th})\beta\eta_p}, u_c = \frac{R_r^{th}}{(\varphi_r)\beta\eta_p}$ and

$$\theta_1 = \frac{m_{ps}}{\Omega_{ps}}, \theta_2 = \frac{m_r}{\Omega_r} + \frac{m_s\phi_3}{\Omega_s}$$

$$\phi_1 = \frac{R_2^{th}}{(\varphi_2 - \varphi_1 R_2^{th})\eta_p}, \phi_2 = \frac{\left(\frac{u_a}{u_b}\right) - 1}{\varphi_2\beta\eta_p}, \phi_3 = u_b\varphi_2\beta\eta_p$$

$$\zeta_1 = \frac{m_r\phi_2}{\Omega_r}, \zeta_2 = \left(\frac{m_s u_b}{\Omega_s} + \frac{m_r\phi_2}{\Omega_r} + \frac{m_s\phi_2\phi_3}{\Omega_s}\right), \zeta_3 = \frac{m_s u_a}{\Omega_s}, \zeta_4 = \left(\frac{m_s u_a}{\Omega_s} + \frac{m_r\phi_2}{\Omega_r}\right)$$

Moreover, when $R_2^{th} \geq \frac{\varphi_2}{\varphi_1}$ and $R_r^{th} \geq \frac{\varphi_r}{\lambda\,\varphi_2}$, $P_{out,sr}^{t_2,}$ becomes unity for both ipSIC and pSIC cases.

2.3.3. System Throughput:

The system throughput is one of the important performance measures to assess the proposed system spectrum utilization. In the case of cooperative communication based wireless networks, it implies the mean spectral efficiency. For the proposed SWIPT based NOMA-CDRT system, it can be defined as the sum of individual target rates for both primary and secondary communications that can be achieved successfully over the Nakagami-*m* fading channels. From the obtained OP expressions, system throughput can be formulated as

$$S_T = \frac{1-\alpha}{2}\left[\left(1 - P_{out,UE1}^{t1}\right)R_1 + \left(1 - P_{out,UE1}^{t2}\right)R_1 + \left(1 - P_{out,UE}^{t2}\right)R_2 + \left(1 - P_{out,sr}^{t2}\right)R_r\right]. \tag{2.37}$$

2.3.4. Energy Efficiency:

The EE of the proposed system can be evaluated using the throughput expression in Eq. (2.37). We measure EE as the ratio of total data delivered to total energy consumed. Here, total amount of data delivered is given by system throughput and the corresponding expression for EE of the considered SWIPT based CDRT-NOMA system model can be given as

$$E_E = \frac{S_T}{\frac{P_p}{2}(1+\alpha)}. \tag{2.38}$$

where S_T is the achievable throughput as expressed in Eq. (2.37).

2.4. Numerical and Simulation Results:

In this section, the simulation and analytical results of SWIPT enabled IoT based CDRT-CNOMA system were presented and the correctness of analytical results was verified with the simulation results using Monte-Carlo simulations. Here, we set the following parameters: $\Omega_{p1} = \Omega_{sr} = 16$, $\Omega_{ps} = \Omega_{s1} = \Omega_{s2} = 1$ as average power of the multipath components, α = 0.2 as the TS factor, the energy conversion efficiency η = 0.7, the PAF as $\psi_1 = \psi_r$ = 0.3, ψ_2 = 0.7, ψ_1^{t2}= 1, $\eta_p$as the SNR, σ^2= 1, and duration of block as T = 1, unless otherwise defined.

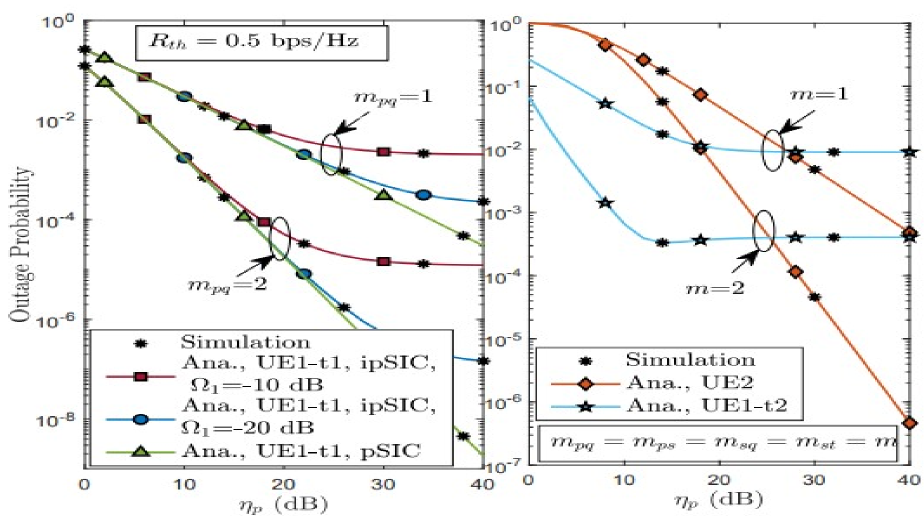

Fig. 2.3: OP versus SNR plots for the primary network with varying m-parameter

In Fig. 2.3, the outage performance of UE1 and UE2 are plotted against the transmit SNR (η_p) in dB for both pSIC and ipSIC cases. Here, we considered fixed data rates $R_1 = R_2 = R_{th} = 0.5$ bps/Hz, with varying fading severity parameter (m-parameter). For the UE1 in IT phase 1, the impact of ipSIC on the OP is shown by varying **Ω**1 = −10, −20 dB. One can observe from the plot, as the m-parameter increases, outage performance improves, unlike the above observations, as a level of ipSIC **Ω**1 increases, outage performance deteriorates. In addition to this, it can be seen that as the η_p increases, outage performance improves for the UE2 and UE1 (pSIC), but for the UE1 (ipSIC) in the IT phase1 and in IT phase 2, it gets outage floor particular in the high range of SNR. This is because the UE1 experiences interference during SIC in IT phase 1 and receives interference from IoT-relay in IT phase 2 owing to the simultaneous transmissions from node PT and ST. From the figure, it is also found that UE2 outperforms UE1 by considering same set of parameters which is obvious because higher power allocation for UE2 and adopting the NOMA principle in the second stage of transmission.

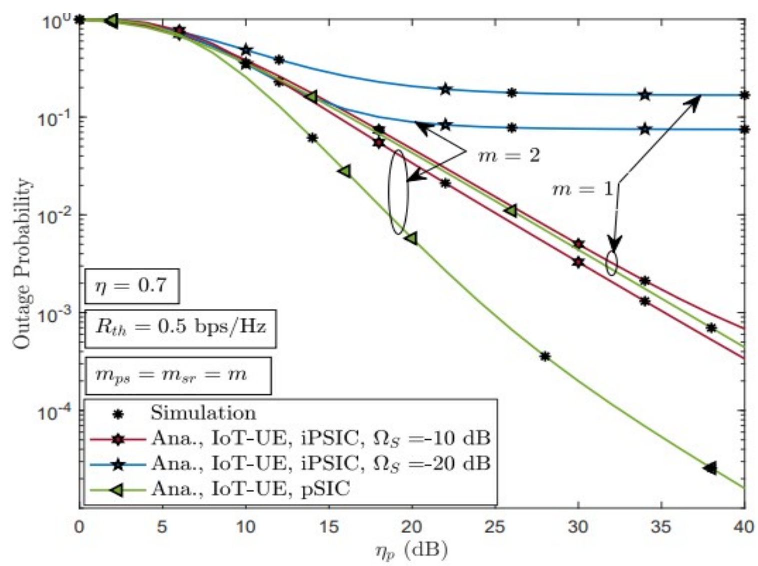

Fig. 2.4: OP versus SNR of IoT-U

Fig. 2.4 demonstrates the OP curve of the IoT-U plotted against η_p for both the cases pSIC and ipSIC. Herein, we set the data rate $R_2 = R_r = R_{th}$= 0.5 with λ = 1 for ipSIC case. As one can observe from the figure, the outage performance of the IoT-U is improved as m-parameter increases from 1 to 2 unlike the impact of ipSIC level **Ω**s changes from -10 dB to -

20 dB. The impact of ipSIC level on outage performance can also be observed from the figure when Ωr vary from -10 dB to -20 dB, it improves the performance. The outage floor for Ωr = −20 dB occurs at comparatively lower SNR than Ωr = −10 dB because of an increase in residual interference and it degrades the performance. However, no outage floor occurs for the pSIC case absence of residual interference and it outperforms ipSIC case.

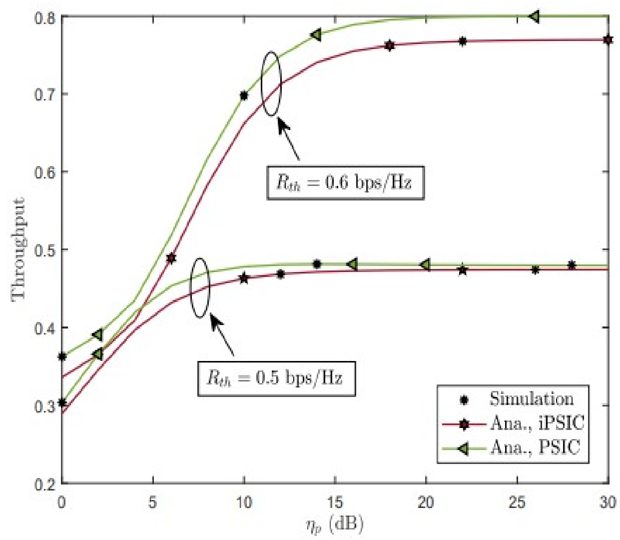

Fig. 2.5: System throughput

Fig. 2.5 shows the impact of SNR on system throughput for both the cases ipSIC and pSIC under the parameter setting as $R_1 = R_2 = R_r = R_{th}$= (0.5, 0.6) bps/Hz, with all m-parameter equal to 2 and Ω1 = Ωr = −20 dB. It can seen from the figure, the system throughput increases for lower to medium range of SNR, but after that it gets saturated, which is its maximum attainable throughput for the specific data rate. For higher data rate, it attains its maximum at relatively high SNR. It happens because the outage performance at a higher target rate is relatively poorer than the lower target rate.

Fig. 2.6 plots the curve for EE versus SNR for both the cases ipSIC and pSIC under the same set of parameters used in Fig. 2.4. Here, one can observe that the maximum EE attains at a specific SNR for given target rate. It changes when we change the target rate. Further, high SNR regions exhibit the lowest EE because, at high SNR, energy consumption is more than the achieved system throughput.

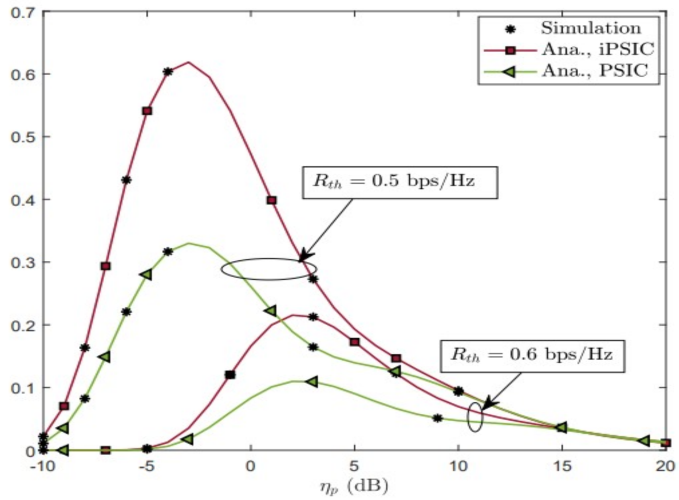

Fig. 2.6: Energy efficiency of CDRT - CNOMA System

2.5. Conclusion:

In this chapter, we proposed and investigated a SWIPT enabled IoT-based CDRT- CNOMA system that improves spectrum utilization and EE. The proposed system performance is evaluated and analysed interms of OP. To know more details of this proposed network along with OP, throughput and EE are also evaluated and the correctness of the results verified with Monte Carlo simulations. The impact of different parameters are also studied on the proposed system. Numerical results emphasized the importance of employing SWIPT enabled IoT relay which provides self-reliant energy efficient communication and data transmission.

Chapter 3

Exploiting Cache-Free/ Cache-Aided SWIPT CDRT-NOMA System Model

3.1. Introduction:

Wireless caching is an important technique used in present and future wireless networks. Caching at the wireless edge is a unique way of boosting spectral efficiency and reduces energy consumption of wireless systems. The performance of cache-aided simultaneous wireless information and power transfer (SWIPT) NOMA - CDRT systems, in which source or base station communicates with far users by the use of relay. To increase the relay serving time, the relay is assumed to be incorporated with a caching and an energy harvesting (EH) capability. On the basis of power-splitting mechanism, the effect of caching on the system performance measures analysed in terms of the system throughput and the energy efficiency (EE).

3.2. System Model:

3.2.1 Description:

The proposed system model is same as previous one, in addition to that we incorporate cache memory in relay node along with EH capability. The advantage of using cache at relay node is that we can reduce the data access delay. This caching scheme can actively pre-fetches the contents from base station or server during off-peak hours and serve the users that can help in the reduction of data access delay. Here, we try to improve the secondary user transmission rate under the constraint of primary user transmission rate.

In Fig. 3.1, we assume that there is a content caching cooperation between primary and secondary networks. Here, we consider a primary system that consists one BS and two PU namely primary near user UE1, primary far user UE2 and also considers a secondary network that consists single IoT-U and a relay node which acts as secondary transmitter (ST). In cache free system model we ignore the cache memory block in relay node i.e., in cache free system model relay is equipped with only EH capability.

All the nodes are equipped with half duplex mode. Along with that, we consider that the relay is equipped with limited cache capacity to store the primary and secondary content. Hence, the relay can simultaneously serve PUs and SUs with appropriate power using ZFBF[35, 36].

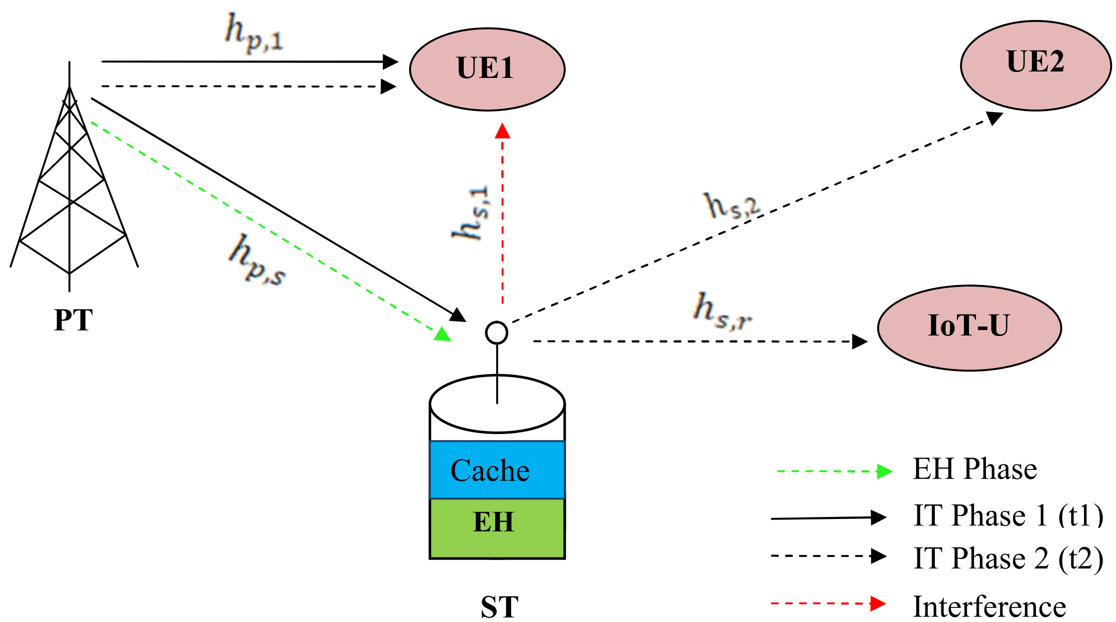

Fig. 3.1: Proposed SWIPT based NOMA-CDRT system with cache for a single cluster

The relay i.e., ST node is considered capable of sensing the spectrum environment. When the primary transmitter (PT) or BS is silent and unable to serve primary users, the licensed spectrum that belongs to the primary network can be shared to the secondary network. Here, all the channels are assumed to be Rayleigh fading channels.

PSC protocol is implemented in this system for EH and information transmission (IT) as shown in Fig. 3.2. In this PS protocol, the transmission block time T is divided into two parts with $\phi \in (0, 1)$ denoting the PSC parameter. Here, first time phase $T/2$ is divided into three sub-parts based on power splitting factor ϕ. In the first $T/2$ time, base station sends information to both UE1 and relay node by exploiting NOMA principle and relay node harvests the energy from base station by utilizing some part of received signal with a part of ϕP_p.

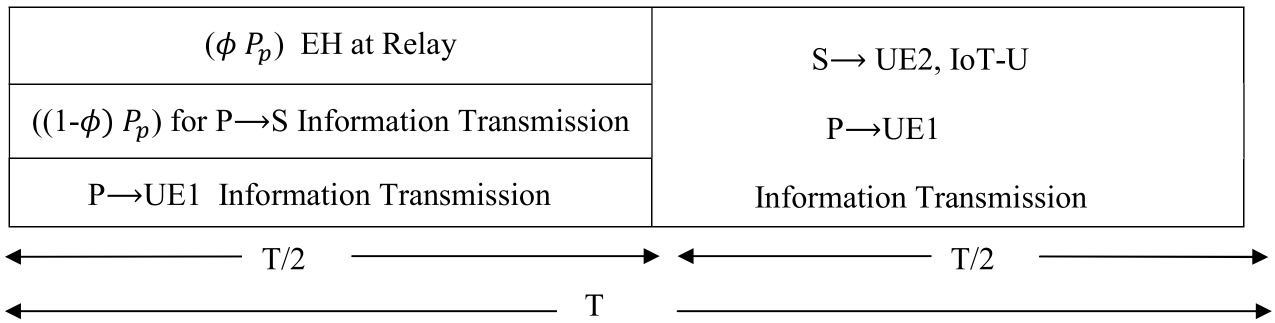

Fig. 3.2: Power splitting protocol with EH and IT Phases

And the next $(1-\phi)P_p$ is used for the information transmission to relay in $T/2$ time. As the information is already sent to relay it is not required to transmit the information in the second phase. Moreover, by implementing caching scheme at relay it may be required to send a new information from source to relay in second time phase. Here, we assume that cache can able to pre-fetch some content from source during off-peak hours. If the requested files of primary and secondary users are not cached in a cache then source will send information to relay in second time phase. During second phase relay will send its information to UE1, UE2 and IoT-U respectively.

3.3. Cache Free SWIPT System Model:

In this model, we ignore the cache memory and follow NOMA- CDRT using power splitting protocol which is similar to the work done in chapter 2.

3.3.1. Energy Harvesting (EH) Phase :

The harvested energy at ST during EH phase is given

$$E_h = \eta \, \phi \, P_P |h_{p,s}|^2 \, T/2, \tag{3.1}$$

where $\eta \in (0,1)$ is the energy conversion efficiency and it depends on the EH circuitry and on the rectification process and P_P is the source transmit power. Hence, the power transmitted from node S over the time *T /2* can be calculated as

$$P_s = \frac{E_h}{T/2} = \eta \, \phi \, P_P |h_{p,s}|^2. \tag{3.2}$$

3.3.2. Information Transmission (IT) Phase:

In the proposed system model overall information transmission takes place in two phases and every phase requires one time slot. In both phases NOMA transmission technique is being employed. IT Phase 1 is denoted as t1, and IT Phase 2 denoted as t2.

During t1 phase, BS transmits its composite signal $X_p = \sqrt{\psi_1 P_p} x_1 + \sqrt{\psi_2 P_p} x_2$ to node UE1 using downlink NOMA transmission principle. Here, ψ_1 and x_1 are power allocation factor and data symbol related to UE1 whereas ψ_2 and x_2 are the power allocation factor and data symbol related to UE2 respectively and assuming x_2 as high powered symbol compared to x_1 thus, we can write $\psi_2 > \psi_1$ and $\psi_1 + \psi_2 = 1$. Thus, the received signals at node j, j ∈ (1,s) can be given as

$$y_{(p,1)} = X_p h_{p,1} + n_{p,1}\,, \tag{3.3}$$

and the signal received at relay node is given by

$$y_{(p,s)} = \left(\sqrt{(1-\phi)\psi_1 P_p} x_1 + \sqrt{(1-\phi)\psi_2 P_p} x_2\right) h_{p,1} + n_{ps}\,, \tag{3.4}$$

where $n_{p,j}$ is the AWGN variable with variance σ^2. Considering the NOMA principle, UE1 performs SIC to decode the x_1 symbol. Initially, UE1 decodes x_2 symbol assuming x_1 as noise and then, after performing SIC, x_1 symbol is decoded at UE1. Hence, the SINR received at UE1 to decode x_2 can be expressed as

$$\gamma^{t_1}_{x_2 \to p,1} = \frac{\psi_2 \, \eta_p |h_{p,1}|^2}{\psi_1 \eta_p |h_{p,1}|^2 + 1}\,, \tag{3.5}$$

and UE1 to decode x_1 can be given as

$$\gamma_{p,1}^{t_1} = \frac{\psi_1 \eta_p |h_{p,1}|^2}{\lambda\, \psi_2 \eta_p |h_{p,1}|^2 + 1}, \tag{3.6}$$

where $\eta_p = \frac{P_P}{\sigma^2}$ is the transmit SNR at primary transmitter and $\boldsymbol{\lambda}$ $(0 < \boldsymbol{\lambda} < 1)$ is the residual interference parameter when $\boldsymbol{\lambda}$=0 it represents pSIC.

Moreover, IoT-relay will decode x_2 symbol by assuming x_1 as noise since it is a low powered symbol. Thus, the received SINR at IoT- relay node is given by

$$\gamma_{p,s}^{t_1} = \frac{(1-\phi)\psi_2 \eta_p |h_{p,s}|^2}{(1-\phi)\psi_1 \eta_p |h_{p,s}|^2 + 1}. \tag{3.7}$$

In the next IT phase 2 (t2), if ST is able to decode symbol x_2 at t1 then only secondary transmission will take place, otherwise ST will remain silent and no transmission takes place during this phase.

Following successful decoding of x_2 at node ST, it combines x_2 with its own signal x_r to create a composite signal $X_s = \sqrt{\psi_2 P_s} x_2 + \sqrt{\psi_r P_s} x_r$ by using NOMA principle, where ψ_2 and x_2 are power allocation coefficient and data symbol related to UE2 whereas ψ_r and x_r are the power allocation coefficient and data symbol related to IoT-U respectively and assuming x_2 as high powered symbol compared to x_r thus, we can write $\psi_2 > \psi_r$ and ψ_2+ ψ_r= 1. Thus, the received signal at UE2 and IoT-U can be given as

$$y_{sj} = X_s h_{s,j} + n_{s,j}, \tag{3.8}$$

where $n_{s,j}$ is the AWGN variable and $j \in$ (2,r). Here, x_2 can be directly decoded at UE2 because of high power allocation, whereas SIC is employed to decode x_r at IoT-U. It first decodes x_2 considering x_r as noise and then decodes x_r by discarding x_2 using SIC. Therefore, the SINR received at UE2 to decode x_2 can be given as

$$\gamma_{s,2}^{t_1} = \frac{\psi_2 \delta\, \eta_p |h_{p,s}|^2 |h_{s,2}|^2}{\psi_r\, \delta\, \eta_p |h_{p,s}|^2 |h_{s,2}|^2 + 1}, \tag{3.9}$$

where $\delta = \eta\, \phi$.

For the secondary network, the received SINR at SR to decode x_2 before decoding x_r is given by

$$\gamma_{x_2 \rightarrow s.r}^{t_2} = \frac{\psi_2 \delta\, \eta_p |h_{p,s}|^2 |h_{s,r}|^2}{\psi_r \delta\, \eta_p |h_{p,s}|^2 |h_{s,r}|^2 + 1}, \tag{3.10}$$

The received SINR at IoT-U to decode x_r after SIC can be given as

$$\gamma_{s,r}^{t_2} = \frac{\psi_r \delta\, \eta_p |h_{p,s}|^2 |h_{s,r}|^2}{\lambda\, \psi_2 \delta\, \eta_p |h_{p,s}|^2 |h_{s,r}|^2 + 1}, \tag{3.11}$$

In order to maximize spectral utilization and the wireless channel, source node PT transmits the new signal $\hat{x}_1$ to UE1 with transmit power $\sqrt{\psi_1^{t_2} P_p}$, $\psi_1^{t_2} \in (0, 1)$. However, during t2, UE1 faces the interference from IoT-relay node ST, which can be estimated and eliminated by using the side information of x_2 that is obtained through SIC process during t1.

Therefore, the signal received at UE1 during t2 is given by

$$y_{(p,s),1}^{t_2} = \sqrt{\psi_1^{t_2} P_p}\, h_{p,1} \hat{x}_1 + h_{s,1} X_s + n_{p,1}, \tag{3.12}$$

and corresponding SINR is given, respectively, by

$$\gamma_{p,1}^{t_2} = \frac{\psi_1^{t2} \eta_p |h_{p,1}|^2}{\psi_r \delta\, \eta_p |h_{p,s}|^2 |h_{s,1}|^2 + 1}. \tag{3.13}$$

3.4. Performance Analysis:

In this section, the performance of primary and secondary networks is evaluated in terms of their outage probability (OP) by deriving analytical expressions over Rayleigh fading channel. Here, we consider R_1, R_2 and R_r as predefined target rate thresholds for UE1, UE2 and IoT-U respectively.

3.4.1 Outage Probability of Primary Network:

3.4.1.1 Outage Probability of UE1:

During t1 phase, the outage event of primary user1 occurs when UE1 unable to decode both symbols x_1 and x_2, and this is given as

$$P_{out,(1,p)}^{t_1,ipSIC} = 1 - P_r\left(\gamma_{x_2\to p,1}^{t_1} > R_2^{th} \,;\, \gamma_{p,1}^{t_1} > R_1^{th}\right). \tag{3.14}$$

where $R_1^{th} = 2^{2R_1} - 1\,, R_2^{th} = 2^{2R_2} - 1$

Now, we evaluate above Eq. (3.14) in both ipSIC and pSIC cases considering $R_2^{th} < \frac{\varphi_2}{\varphi_1}$ into account in the following sections.

a) ipSIC: $P_{out,(1,p)}^{t_1,ipSIC}$ for the ipSIC case can be evaluated through following theorem.

Theorem 1: The exact form expression of $P_{out,(1,p)}^{t_1,ipSIC}$ for ipSIC case calculated over Rayleigh fading can be expressed as

$$P_{out,(1,p)}^{t_1,ipSIC} = 1 - P_r\left[|h_{p,1}|^2 > \Delta\right] = Exp\left(-\frac{\Delta}{\Omega_{p1}}\right), \tag{3.15}$$

where $\Delta = max\,(u_1, u_2)$ and $u_1 = \frac{R_2^{th}}{(\varphi_2 - \varphi_1 R_2^{th})\eta_p}$, $u_2 = \frac{R_2^{th}}{(\varphi_1 - \lambda\varphi_2 R_2^{th})\eta_p}$

b) pSIC: Invoking respective SINRs into Eq. (3.15) and considering $\boldsymbol{\lambda}$=0 for pSIC case, we can evaluate Eq. (3.15) as shown below.

$$P_{out,(1,p)}^{t_1,ipSIC} = 1 - P_r\left(|h_{p,1}|^2 > \frac{R_1^{th}}{\varphi_1\eta_p};\, |h_{p,1}|^2 > \frac{R_2^{th}}{(\varphi_2 - \varphi_1 R_2^{th})\eta_p}\right), \tag{3.16}$$

considering $z = |h_{p,1}|^2, u_1 = \frac{R_1^{th}}{\varphi_1\eta_p}, u_2 = \frac{R_2^{th}}{(\varphi_2 - \varphi_1 R_2^{th})\eta_p}$, now Eq. (3.16) can be modified as

$$P_{out,(1,p)}^{t_1,pSIC} = 1 - P_r(z > max\,(u_1, u_2))\,, \tag{3.17}$$

Case i: if $u_1 > u_2$,

$$P_r(z > u_1) = exp^{-\left(\frac{m_{p1}}{\Omega_{p1}}\right)\left(\frac{R_1^{th}}{\varphi_1\eta_p}\right)} \sum_{k=0}^{m_{p1}-1} \frac{\left(\frac{m_{p1}}{\Omega_{p1}}\frac{R_1^{th}}{\varphi_1\eta_p}\right)^k}{k!}, \tag{3.18}$$

Case ii: if $u_1 < u_2$

$$P_r(z > u_2) = exp^{-\left(\frac{m_{p1}}{\Omega_{p1}}\right)(u_2)} \sum_{k=0}^{m_{p1}-1} \frac{\left(\frac{m_{p1}}{\Omega_{p1}} u_2\right)^k}{k!}, \tag{3.19}$$

By substituting Eq. (3.18), Eq. (3.19) in above Eq. (3.17) one can get $P_{out,(1,p)}^{t_1,pSIC}$ for pSIC case.

3.4.1.2. Outage Probability of UE2:

The outage event of the UE2 occurs either UE2 cannot decode its symbol x_2 or the relay node is unsuccessful in decoding. For a predefined target rate R_2 the OP of UE2 is given as below.

$$P_{out,UE2}^{t_2} = \underbrace{P_r\left(\gamma_{p,s}^{t_1} > R_2^{th} \; ; \; \gamma_{s,2}^{t_2} > R_2^{th}\right)}_{P_1} + \underbrace{P_r\left(\gamma_{p,s}^{t_1} < R_2^{th}\right)}_{P_2}. \tag{3.20}$$

By invoking respective SINR model equations into above and performing some mathematical computations on those will result in expressions given in following lemma.

Lemma 2: The analytical expression for $P_{out,UE2}^{t_2}$ over Rayleigh fading channel conditioned on $R_2^{th} < \frac{\varphi_2}{\varphi_1}$ can be given as $P_{out,UE}^{t_2} = P_1 + P_2$. Final expression for $P_{out,UE2}^{t_2}$ is given as

$$P_{out,UE2}^{t_2} = \frac{u_4}{\rho_p \Omega_{ps} \Omega_{s2}} Ei\left[1, \frac{u_3}{\rho_p \Omega_{ps}}\right], \tag{3.21}$$

where $u_3 = \frac{R_2^{th}}{(\varphi_2 - \varphi_1 R_2^{th})\beta\eta_p}$ and $u_4 = \frac{R_2^{th}}{(\varphi_2 - \varphi_r R_2^{th})\beta\eta_p}$.

3.4.2. Outage Probability of Secondary Network:

Secondary transmission takes place only when ST able to decode x_2 symbol, else secondary network will be in outage. For the IoT-U, the outage event occurs either when ST node could not detect symbol x_2 or when IoT- relay node ST unable to detect x_r along with successful detection of x_2.

For a given predefined target rate threshold R_r , the OP of secondary network is given as

$$P_{out,sr}^{t_2} = \underbrace{P_r\left(\gamma_{p,s}^{t_1} > R_2^{th} \,;\, \bar{P}_{sr}\right)}_{P_{out1}} + \underbrace{P_r\left(\gamma_{p,s}^{t_1} < R_2^{th}\right)}_{P_{out2}}. \tag{3.22}$$

where $R_r^{th} = 2^{\frac{2\,\eta\, R_r}{1-\alpha}}$, $\bar{P}_{sr}$ denotes the OP of IoT-U fails to detect any symbol can be given as

$$\bar{P}_{sr} = 1 - P_r\left(\gamma_{x_2 \to s.r}^{t_2} > R_2^{th} \,;\, \gamma_{s,r}^{t_2} > R_r^{th}\right), \tag{3.23}$$

After plugging respective SINRs into Eq.(3.23) and performing some algebraic manipulations, further it can be expressed as follows for ipSIC and pSIC cases, respectively. For pSIC case set $\boldsymbol{\lambda}$=0.

Lemma 3: The analytical expression for $P_{out,UE2}^{t_2}$ over Rayleigh fading channel conditioned on $R_2^{th} < \frac{\varphi_2}{\varphi_r}$ can be given as $P_{out,sr}^{t_2}$. Final expression for $P_{out,UE2}^{t_2}$ is given as

$$P_{out,sr}^{t_2} = \frac{u_c}{\rho_p \Omega_{ps} \Omega_{s2}} Ei\left[1, \frac{u_3}{\rho_p \Omega_{ps}}\right], \tag{3.24}$$

where $u_c = \max(u_5, u_6)$, $u_5 = \frac{R_2^{th}}{(\varphi_2 - \varphi_r R_2^{th})\beta\eta_p}$ and $u_6 = \frac{R_r^{th}}{(\varphi_r - \lambda\varphi_2 R_r^{th})\beta\eta_p}$.

3.5. Cache Aided SWIPT System Model:

Here, in cache aided system model we include cache memory at the relay node and based on the system model we assume that cache is assumed to have limited cache capacity. On the basis of this system model and considering transmission block time (T1) into account we formulate a transmission model which helps in evaluating transmission rate.

3.5.1. Transmission Model:

In the information transmission model, we assume that the available bandwidth is 1MHZ and the time duration that a primary user is allowed to transmit a requested file over bandwidth is T1. In terms of the primary and secondary content cached, a time slot *T/2* is divided into three parts:

$\boldsymbol{t_p}$: It is the time taken by the cache to fetch the un-cached primary content for the PU.

$\boldsymbol{t_s}$**:** It is the time taken by the cache to fetch the un-cached secondary content for the SU.

$\boldsymbol{T_1 - t_p - t_s}$: It indicates the time when the secondary relay node transmits simultaneously the primary and secondary content.

Time required by relay to fetch un-cached primary content for primary user	Time taken by cache in relay node to fetch the un-cached secondary content for secondary user	Time taken by cache in relay node to fetch the un-cached secondary content for secondary user
$\longleftarrow t_p \longrightarrow$	$\longleftarrow t_s \longrightarrow$	$\longleftarrow T_1 - t_p - t_s \longrightarrow$

Fig. 3.3: Time taken by cache memory to fetch un-cached content for PU and SU

Here, we consider that system consists of two networks namely primary and secondary which are interested in different file contents. Let, x_p and x_s are the requested file signals transmitted by BS or ST. And also, relay node allocates a considerable amount of power to serve the primary and its own users. The received signal at primary users (UE1,UE2) and secondary user (IoT-U) are given by

$$y_{(s,j)} = \sqrt{\mu\, h_{s,j} P_s} x_p + n_{s,j}\ , \tag{3.25}$$

Where j={1,2}, similarly the received signal at IoT-U is given by

$$y_{(s,r)} = \sqrt{(1-\mu) h_{s,r} P_s} x_s + n_{s,r}\ , \tag{3.26}$$

where μ and (1-μ) are the power allocation coefficients of primary and secondary users.

Signal to noise ratio (SNR) received at primary and secondary users are given by

$$(SNR)_{PU} = \gamma_{pu} = \frac{\mu\, \eta_s\, |h_{s,j}|^2}{(1-\mu)\, \eta_s\, |h_{s,j}|^2 + 1}, \tag{3.27}$$

$$(SNR)_{SU} = \gamma_{su} = \frac{(1-\mu)\, \eta_s\, |h_{s,j}|^2}{(\mu)\, \eta_s\, |h_{s,j}|^2+1}\,. \tag{3.28}$$

In cache aided system model, we assume that cache in relay can pre-fetch the some popular contents of primary network and secondary network during off-peak hours. Based on the cached content of the primary and secondary users, we categorize the transmission model into 4 types.

Type-1:

When both the primary and secondary files that are requested by the PU and SU are cached in the relay, then relay can serve the PU and SU simultaneously over the whole time in t2 phase (T/2). Thus, the transmission data rate for PU and SU are respectively given as

$$R_1^{pu} = R_p . P_r\big(T_1 log_2(1 + (SNR)_{PU} \geq\ R_{eq}^{th}\big)\,, \tag{3.29}$$

$$R_1^{su} = R_s . P_r\big(T_1 log_2(1 + (SNR)_{SU} \geq\ R_{eq}^{th}\big)\,, \tag{3.30}$$

Output expressions for R_1^{pu} and R_1^{su} can be given as

$$R_1^{pu} = R_p\left(1 - 2\left(\frac{\phi_1 \Omega_{ps}}{\Omega_{s1}}\right)^{\frac{1}{2}} K_1\left(2\sqrt{\frac{\phi_1}{\Omega_{s1}\, \Omega_{ps}}}\right)\right), \tag{3.31}$$

$$R_1^{su} = R_s\left(1 - 2\left(\frac{\phi_1 \Omega_{ps}}{\Omega_{sr}}\right)^{\frac{1}{2}} K_1\left(2\sqrt{\frac{\phi_1}{\Omega_{sr}\, \Omega_{ps}}}\right)\right). \tag{3.32}$$

Proof: Refer Appendix E.

Type-2:

When the requested primary content of primary user is in cache and secondary user IoT-U content is not cached in relay then the transmission rate is given by

$$R_2^{pu} = R_p . P_r\big((T_1 - t_s) log_2(1 + (SNR)_{PU} \geq\ R_{eq}^{th}\big)\,, \tag{3.33}$$

$$R_2^{su} = R_s . P_r\big((T_1 - t_s) log_2(1 + (SNR)_{SU} \geq\ R_{eq}^{th}\big)\,. \tag{3.34}$$

Type-3:

When the requested primary content is not in cached in relay and SU content is cached in relay, then the transmission rate is given by

$$R_3^{pu} = R_p . P_r\big((T_1 - t_p)log_2(1 + (SNR)_{PU} \geq \ R_{eq}^{th}\big) \, , \tag{3.35}$$

$$R_3^{su} = R_s . P_r\big((T_1 - t_p)log_2(1 + (SNR)_{SU} \geq \ R_{eq}^{th}\big) \, . \tag{3.36}$$

Type-4:

When both PU and SU requests are not cached in relay, then the transmission data rate for PU and SU are respectively given by

$$R_4^{pu} = R_p . P_r\big((T_1 - t_p - t_s)log_2(1 + (SNR)_{PU} \geq \ R_{eq}^{th}\big) \, , \tag{3.37}$$

$$R_4^{su} = R_s . P_r\big((T_1 - t_p - t_s)log_2(1 + (SNR)_{SU} \geq \ R_{eq}^{th}\big) \, . \tag{3.38}$$

3.5.2. Caching Model:

Here, we assume that the library of files requested by primary and secondary network users as $F_{PU} \cong \{1,2,3, \dots, M\}$ and $F_{SU} \cong \{1,2,3, \dots, N\}$. Without loss of generality, we suppose that the popularities of primary and secondary content follow the zipf law, which is widely used in Refs. [35,36] are given by

$$f_i^{PU} = \frac{i^{-\gamma_p}}{\sum_{n=1}^{M} n^{-\gamma_p}} \; ; (i \in F_{PU}) \, , \tag{3.39}$$

$$f_j^{SU} = \frac{j^{-\gamma_s}}{\sum_{n=1}^{N} n^{-\gamma_s}} ; (j \in F_{SU}) \, , \tag{3.40}$$

In this model, we assume that the file popularity contents of primary and secondary follow descending order and is shown as $f_1^{PU} \geq f_2^{PU} \geq f_3^{PU} \geq \cdots \geq f_M^{PU}$ and $f_1^{SU} \geq f_2^{SU} \geq f_3^{SU} \geq \cdots \geq f_N^{SU}$ with $\sum_{i=1}^{M} f_i^{PU} = 1$ and $\sum_{j=1}^{N} f_j^{SU} = 1$. As we assume that, cache can access some of the contents during off-peak hours due to this, relay can gain more transmission time and secondary transmitter can able to serve both primary and secondary users simultaneously and can lead to successful transmission of the information in the entire network.

Here, we consider that C as the total cache capacity of relay and C_0 is the amount of capacity used to serve the primary content and remaining portion $C - C_0$ is used to serve its own users.

3.6. Performance Analysis:

3.6.1. Transmission Rate:

To maximize the usage of secondary transmitter, we calculate the effective transmission rates of PU and SU from ST.

$$R^{su}(C_0, \beta) = p_p . p_s . R_1^{su} + p_p . R_2^{su} + p_s . R_3^{su} + R_4^{su} , \tag{3.41}$$

subject to

$$R^{pu}(C_0, \beta) = p_p . p_s . R_1^{pu} + p_p . R_2^{pu} + p_s . R_3^{pu} + R_4^{pu} , \tag{3.42}$$

$$0 \le t_s \le T_1;\ 0 \le t_p \le T_1;\ 0 \le t_p + t_s \le T_1;\ 0 \le C_0 \le C;\ 0 \le \mu \le 1$$

above equations can be re-written as

$$\begin{aligned} R^{su}(q, \beta) = {} & \frac{(lc)^{1-\gamma_p} - 1}{M^{1-\gamma_p} - 1} . \frac{((1-l)c)^{1-\gamma_s} - 1}{M^{1-\gamma_s} - 1} . R_1^{su} + \frac{(lc)^{1-\gamma_p} - 1}{M^{1-\gamma_p} - 1} . R_2^{su} \\ & + \frac{((1-l)c)^{1-\gamma_s} - 1}{M^{1-\gamma_s} - 1} . R_3^{su} + R_4^{su} , \end{aligned} \tag{3.43}$$

$$\begin{aligned} R^{pu}(q, \beta) = {} & \frac{(lc)^{1-\gamma_p} - 1}{M^{1-\gamma_p} - 1} . \frac{((1-l)c)^{1-\gamma_s} - 1}{M^{1-\gamma_s} - 1} . R_1^{pu} + \frac{(lc)^{1-\gamma_p} - 1}{M^{1-\gamma_p} - 1} . R_2^{pu} \\ & + \frac{((1-l)c)^{1-\gamma_s} - 1}{M^{1-\gamma_s} - 1} . R_3^{pu} + R_4^{pu} . \end{aligned} \tag{3.44}$$

where γ_p, γ_s are the primary and secondary file contents popularities and the cumulative distribution function of the file popularity distribution of primary and secondary p_p and p_s following approximation of the sum of zipf probabilities is useful.

$$p_p = \sum_{i=1}^{C_0} f_i^{pu} \cong \frac{{C_0}^{1-\gamma_p} - 1}{M^{1-\gamma_p} - 1}, \tag{3.45}$$

$$p_s = \sum_{i=1}^{C-C_0} f_j^{su} \cong \frac{(C - C_0)^{1-\gamma_s} - 1}{N^{1-\gamma_s} - 1}. \tag{3.46}$$

3.6.2. Outage Probability:

Using cache scheme, outage event of primary user and secondary user occurs in above mentioned four types.

$$(P_{out})_{PU} = p_p . p_s . (P_{out1})_{PU} + p_p . (P_{out2})_{PU} + p_s . (P_{out3})_{PU} + (P_{out4})_{PU}\, , \tag{3.47}$$

$$(P_{out})_{SU} = p_p . p_s . (P_{out1})_{SU} + p_p . (P_{out}\ )_{SU} + p_s . (P_{out3})_{SU} + (P_{out4})_{SU}\, . \tag{3.48}$$

Type-1:

When cache already have the requested file contents of PU and SU, then outage event of PU and SU is given by

$$(P_{out}\ )_{PU} = 1 - P_r\big(T_1 log_2(1 + (SNR)_{PU} \geq\ R_{eq}^{th}\big)\, , \tag{3.49}$$

$$(P_{out1})_{SU} = 1 - P_r\big(T_1 log_2(1 + (SNR)_{SU} \geq\ R_{eq}^{th}\big)\, . \tag{3.50}$$

Output expressions for $(P_{out1})_{PU}$ and $(P_{out1})_{SU}$ can be given as

$$(P_{out1})_{PU} = 1 - \left(1 - 2\left(\frac{\Phi_1 \Omega_{ps}}{\Omega_{s1}}\right)^{\frac{1}{2}} K_1\left(2\sqrt{\frac{\Phi_1}{\Omega_{s1}\, \Omega_{ps}}} \right) \right), \tag{3.51}$$

$$(P_{out1})_{SU} = 1 - \left(1 - 2\left(\frac{\Phi_1 \Omega_{ps}}{\Omega_{s1}}\right)^{\frac{1}{2}} K_1\left(2\sqrt{\frac{\Phi_1}{\Omega_{s1}\, \Omega_{ps}}} \right) \right). \tag{3.52}$$

Note: Proof of $(P_{out1})_{PU}$ and $(P_{out1})_{SU}$ is similar to R_1^{pu} and R_1^{su}.

Type-2:

When cache has to fetch the requested file content of SU during t_s time, then its outage is given by

$$(P_{out2})_{PU} = 1 - P_r\big((T_1 - t_s)log_2(1 + (SNR)_{PU} \geq \ R_{eq}^{th}\big)\,, \tag{3.53}$$

$$(P_{out2})_{SU} = 1 - P_r\big((T_1 - t_s)log_2(1 + (SNR)_{SU} \geq \ R_{eq}^{th}\big)\,. \tag{3.54}$$

Note: Output expressions and proof is similar to type-1 OP by replacing T_1 with $T_1 - t_s$.

Type-3:

When cache has to fetch the requested file content of PU during t_p time, then its outage is given by

$$(P_{out3})_{PU} = 1 - P_r\big((T_1 - t_p)log_2(1 + (SNR)_{PU} \geq \ R_{eq}^{th}\big)\,, \tag{3.55}$$

$$(P_{out3})_{SU} = 1 - P_r\big((T_1 - t_p)log_2(1 + (SNR)_{SU} \geq \ R_{eq}^{th}\big)\,. \tag{3.56}$$

Note: Output expressions and Proof is similar to type-1 OP by replacing T_1 with $T_1 - t_p$.

Type-4:

When cache has to fetch the requested file contents of PU and SU during t_p and t_s time, then its outage is given by

$$(P_{out4})_{PU} = 1 - P_r\big((T_1 - t_p - t_s)log_2(1 + (SNR)_{PU} \geq \ R_{eq}^{th}\big)\,, \tag{3.57}$$

$$(P_{out4})_{SU} = 1 - P_r\big((T_1 - t_p - t_s)log_2(1 + (SNR)_{SU} \geq \ R_{eq}^{th}\big)\,. \tag{3.58}$$

Note: Output expressions and proof is similar to type-1 OP by replacing T_1 with $T_1 - t_p - t_s$.

3.6.3. System Throughput:

One of the important key measures to assess the spectrum utilization is the system throughput. It is considered as the mean spectral efficiency in the case of cooperative communication based wireless networks. For the proposed cache free/cache aided SWIPT based NOMA-CDRT system, it can be given as the sum of individual target rates for both primary and secondary communications that can be achieved successfully over the Rayleigh fading channels. From the derived OP expressions, system throughput can be formulated as

$$S_T = \tfrac{1}{2}\big[(1 - (P_{out})_{PU})R_{pu} + (1 - (P_{out})_{SU})R_{su}\big]\,. \tag{3.59}$$

where R_{pu} and R_{su} are the predefined data rates for PU and SU respectively.

3.6.4 Energy Efficiency:

For the proposed system, the EE can be evaluated using the throughput expression in Eq. (3.59). We measure EE as the ratio of total amount of data delivered to total energy consumed. Here, total amount of data delivered is given by system throughput and the corresponding expression for energy efficiency of the considered cache free/cache aided SWIPT based CDRT-NOMA system model can be given as

$$E_E = \frac{2\, S_T}{\eta_p}. \tag{3.60}$$

Where S_T is the achievable throughput.

3.7 Numerical and Simulation Results:

In this section, we present the numerical and simulation results of cache free and cache enabled SWIPT system and also we verified the correctness of analytical results with Monte-Carlo simulations. The parameters that we considered here are given as: $\Omega_{p1} = \Omega_{sr} = 16$, $\Omega_{ps} = \Omega_{s1} = \Omega_{s2} = 1$ as average power of the multipath components, ϕ = 0.2 as the PS factor, the energy conversion efficiency η = 0.7, the PAF as $\psi_1 = \psi_r$ = 0.3, ψ_2 = 0.7, ψ_1^{t2}= 1, $\eta_p$as the SNR, σ^2= 1, and duration of block as T = 1, Number of files for primary and secondary users respectively given as M=500, N=200 and cache capacity C=200, unless otherwise stated.

In Fig. 3.4 and Fig. 3.5 zipf probability distribution curve for primary and secondary files is plotted by considering primary and secondary file popularities into the account. Here, we can observe that less number of files will have more file popularity. Hence, more popularity files are usually less in number.

In Fig. 3.6, we have plotted the transmission rate of PU and SU for their own content as a function of content caching portion for three different combinations of γ_p and γ_s respectively. For the PU as γ_p increases, transmission rate increases to a considerable amount because the PU's most popular content is increased more when there is a increase in file popularity. In the similar way, for the secondary user IoT-U as γ_s increases, we can achieve more increase in transmission rate.

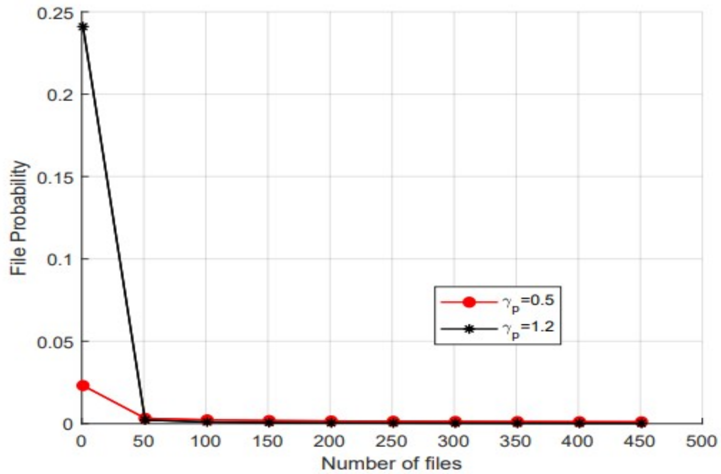

Fig. 3.4: Zipf probability distribution curve for primary user

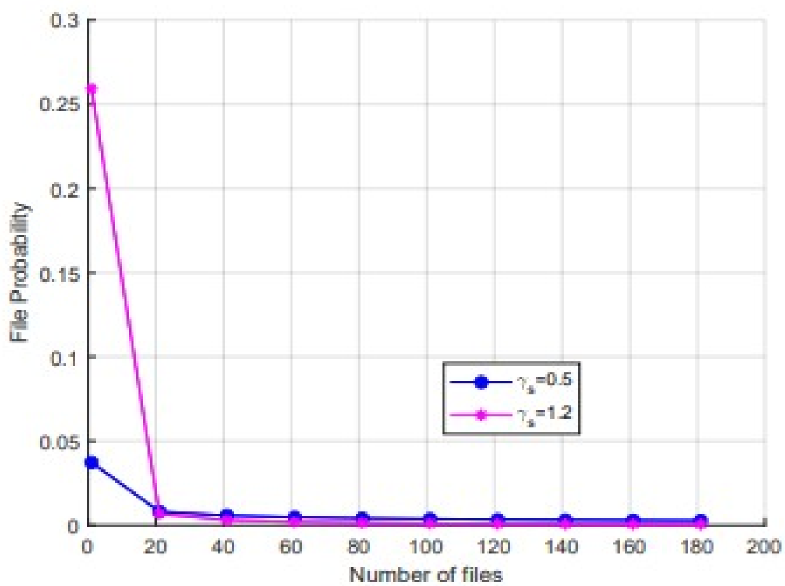

Fig. 3.5: Zipf probability distribution curve for secondary user

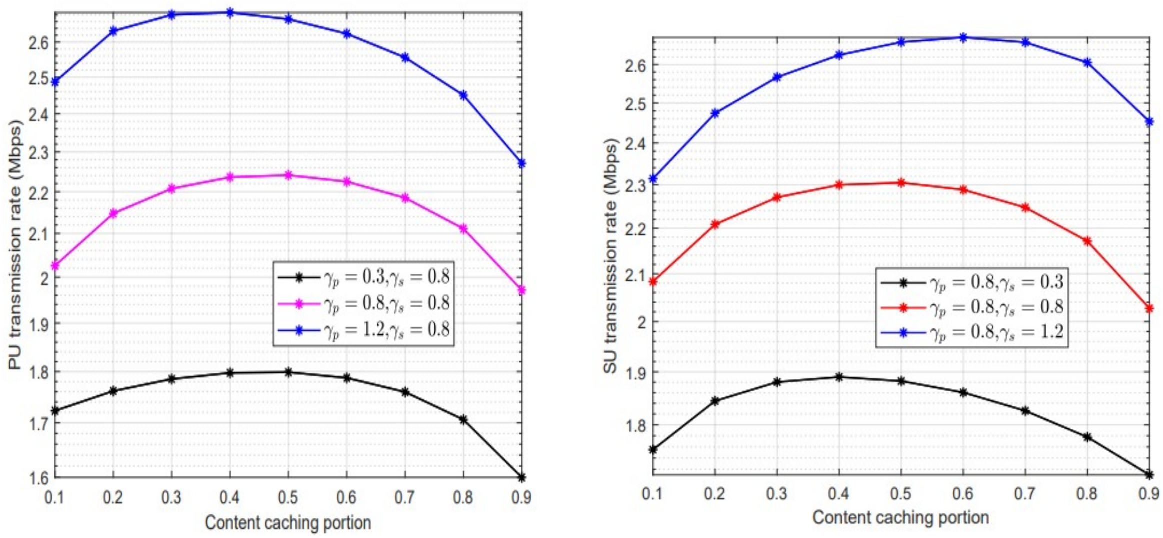

Fig. 3.6: Content caching portion versus PU, SU transmission rate

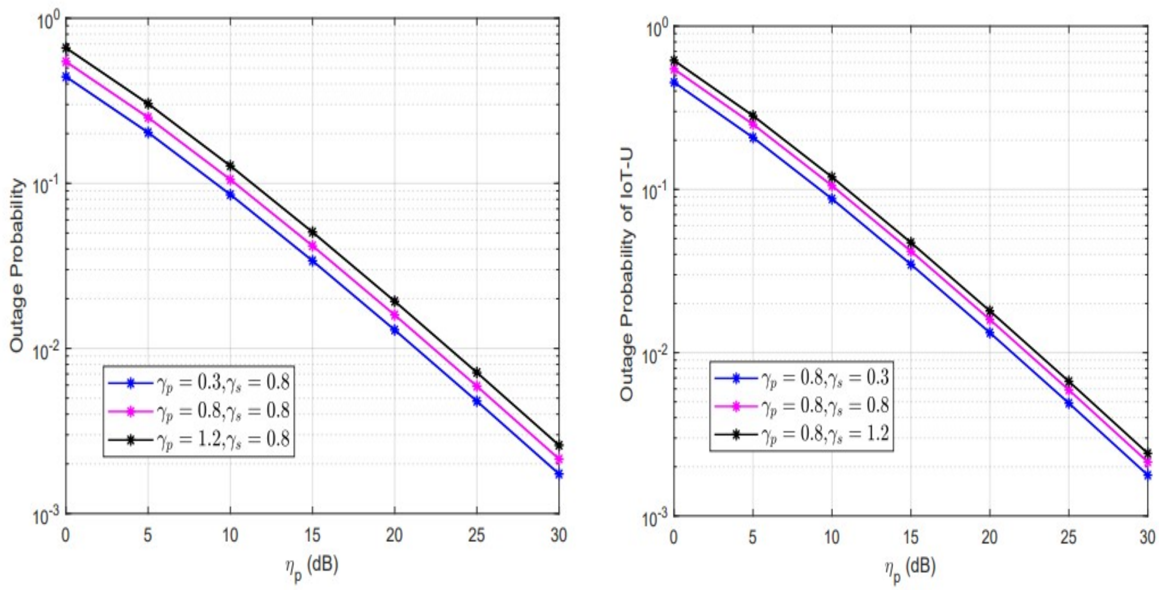

Fig. 3.7: OP of PU and SU versus transmit SNR $\eta_p(dB)$

In Fig. 3.7, we analysed the system performance in terms of OP, as the η_p(dB) increases the OP decreases for both primary and IoT-U and also we can observe that as the file popularity is decreasing there will be a better performance in OP.

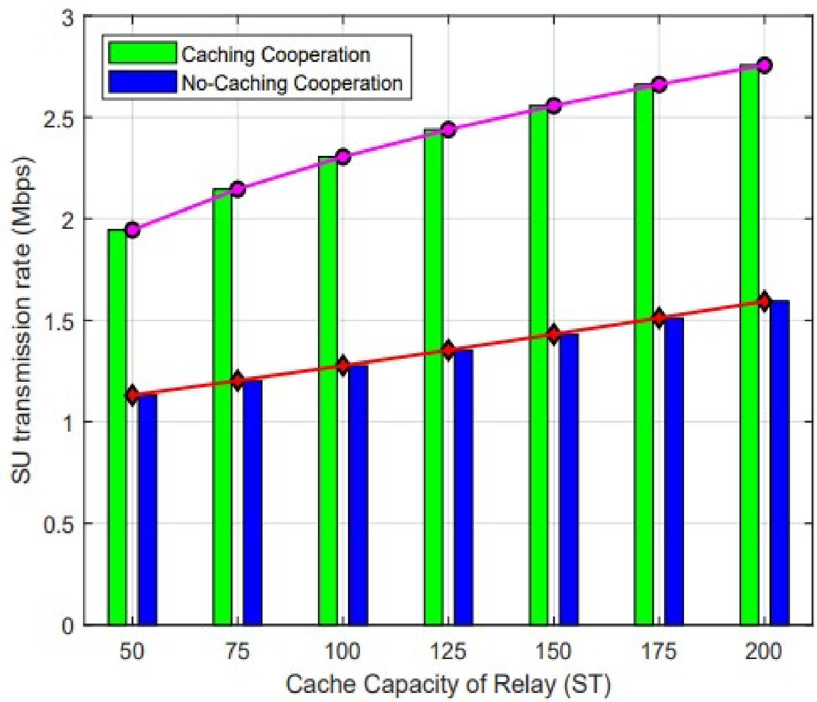

Fig.3.8: Effective achievable transmission rates for different cache capacity

Fig. 3.8, shows the impact of different cache capacities on achievable transmission rate of IoT-U. We can expect more SU transmission rate as the C increases, because as we increase C then we can expect more requested content for PU and SU can be transmitted simultaneously, thus we can reduce transmission delay. Cache aided system model provides higher transmission rate compared to cache free system model as shown in Fig. 3.8.

In Fig. 3.9, effective transmission rate of secondary user increases as transmit power increases, compared to non caching scheme, cache scheme will provide more transmission rate. When the transmitted power is increased the primary network reduces the dependency on content caching cooperation so that additional power can be used for SU transmission.

In Fig. 3.10, depicts that as the data rate increasing we could able to observe the improvement in system throughput. Here, we set the data rates $R_1 = R_2 = R_r = 0.5, 0.6\ bps/Hz$. It can be seen from the figure, for lower to medium range of SNR the system throughput increases, but after that it gets saturated, which is its maximum attainable throughput for the specific data rate. For higher data rate, it attains its maximum at relatively high SNR. It happens because the outage performance at a higher target rate is relatively poorer than the lower target rate.

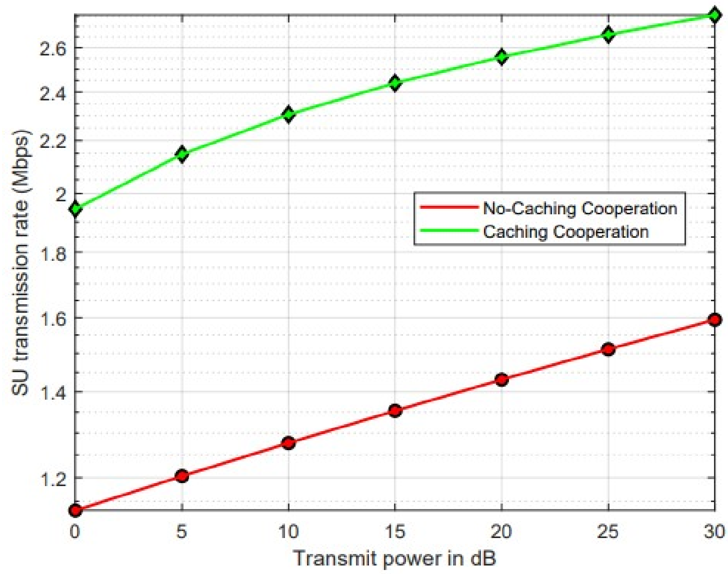

Fig. 3.9: IoT-U transmission rate versus transmit power with and without caching scheme

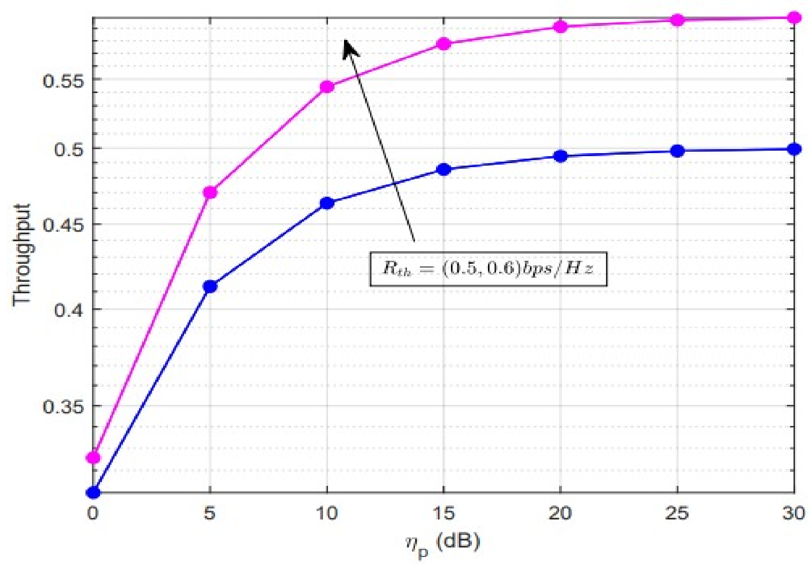

Fig. 3.10: Throughput versus $\eta_p(dB)$

In Fig. 3.11, one can observe that for a given target rate, the maximum EE attains at a specific SNR.

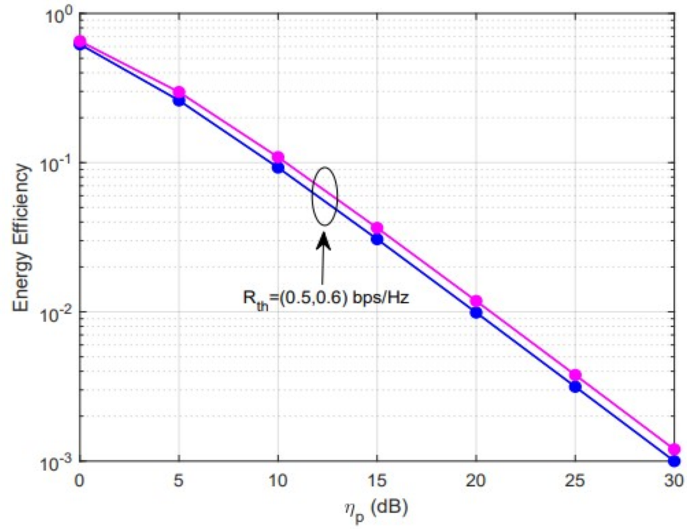

Fig. 3.11: Energy efficiency versus $\eta_p(dB)$

It changes when we change the target rate. Further, high SNR regions exhibit the lowest energy efficiency because, at high SNR, energy consumption is more than the achieved system throughput.

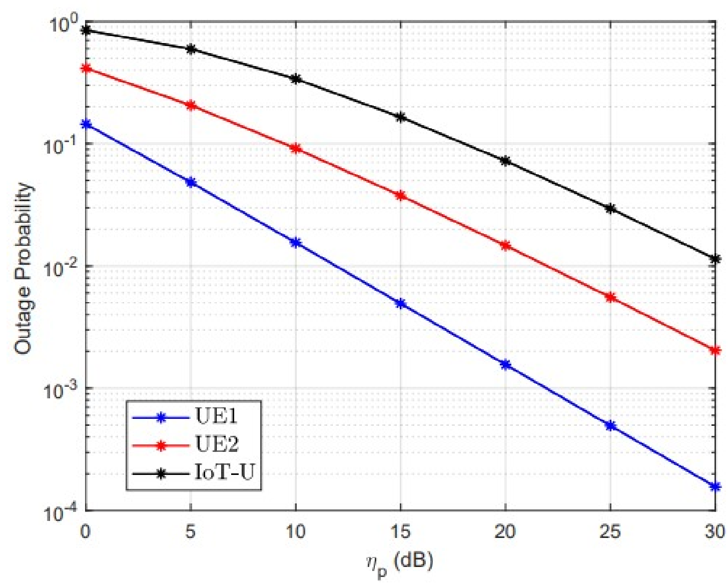

Fig. 3.12: OP of SWIPT based NOMA CDRT system over Rayleigh fading channel

In Fig. 3.12, we have plotted the OP of SWIPT based NOMA CDRT system over Rayleigh fading channel by using power splitting protocol without using caching scheme. Here, as

SNR increases, OP decreases indicates as signal power increases there will be a better performance from the system.

3.8. Conclusion:

In this chapter, we proposed and analysed the system performance of cache free/cache aided SWIPT based CDRT-NOMA system performance that improves spectrum utilization and EE. The proposed system performance is evaluated and analysed interms of OP. To know more details of this proposed network along with OP, throughput and EE are also evaluated and the correctness of the results verified with Monte Carlo simulations. The impact of different parameters are also studied on the proposed system. Simulation results show that there is a great improvement in the transmission rate performance with caching cooperation.

Chapter 4

Conclusion and Future Scope

4.1 Conclusion:

In this work, SWIPT enabled NOMA-CDRT using TSC protocol over Nakagami-*m* fading channel is studied. The performance of the proposed system is evaluated and analysed in terms of outage probability. To know more details of this proposed network along with outage probability, throughput and energy efficiency are also evaluated and the correctness of the results verified with Monte Carlo simulations. On the performance of SWIPT enabled NOMA-CDRT, the impact of different parameters are also studied. Numerical results emphasized the importance of employing SWIPT enabled IoT relay which provides self-reliant energy efficient communication and data transmission. We also implemented caching cooperation scheme in SWIPT model with power splitting protocol that reduces the data access delay time and improved the transmission rate performance. We also calculated the outage probability, system throughput and energy efficiency using cache model under Rayleigh-fading channel that provided a proper comparison between caching and non caching cooperation schemes.

4.2 Future Scope:

In the proposed system model, the investigation for multi-antenna node, full-duplex, non-linear EH model, and the ESC arise as a potential future work. In addition to this, in the caching model the prediction of file popularity can be done with the help of machine learning and big data methods. Nevertheless, the outcomes of this research will be used as a benchmark and provide the guidelines for the design of futuristic 5G wireless communication.

APPENDIX

Appendix A:

By invoking Eq. (2.4) and Eq. (2.5) in Eq. (2.13), can be expressed as

$$P_{out,UE1}^{t1} = 1 - P_r\left(\frac{\psi_2\,\eta_p|h_{p,1}|^2}{\psi_1\eta_p|h_{p,1}|^2 + 1} > R_2^{th}\,;\,\frac{\psi_1\eta_p|h_{p,1}|^2}{\lambda\,\psi_2\eta_p|\hat{h}_{p,1}|^2 + 1} > \ R_1^{th}\right), \quad (1)$$

Performing some algebraic manipulations and rewriting above given as

$$P_{out,UE1}^{t1} = 1 - P_r\left(|h_{p,1}|^2 > u_2\,;|h_{p,1}|^2 > u_3\left(\psi_2\eta_p|\hat{h}_{p,1}|^2 + 1\right)\right), \quad (2)$$

$$= 1 - P_r\left(\left|h_{p,1}\right|^2 > max\left(u_2; u_3\ \left(\psi_2\eta_p\left|\hat{h}_{p,1}\right|^2 + 1\right)\right)\right),$$

$$= 1 - \underbrace{P_r\left(|h_{p,1}|^2 > \ u_3\,;\,u_3\left(\psi_2\eta_p\left|\hat{h}_{p,1}\right|^2 + 1\right) < u_2\right)}_{Z_1}$$

$$- \underbrace{P_r\left(|h_{p,1}|^2 > \ u_3\left(\psi_2\eta_p|\hat{h}_{p,1}|^2 + 1\right);\,u_3\left(\psi_2\eta_p|\hat{h}_{p,1}|^2 + 1\right) > u_2\right)}_{Z_0}, \quad (3)$$

where $u_3 = \frac{R_1^{th}}{\varphi_1\eta_p}$, $u_2 = \frac{R_2^{th}}{(\varphi_2 - \varphi_1 R_2^{th})\eta_p}$ and assuming $|h_{p,1}|^2 \cong X, |\hat{h}_{p,1}|^2 \cong Y$, Z_1 and Z_0 can be further evaluated as

$$Z_1 = \ \bar{F}_X(u_2)F_Y(U)\,, \quad (4)$$

$$Z_0 = \int_U^\infty\left(\int_{u_3\left(\psi_2\eta_p\left|\hat{h}_{p,1}\right|^2+1\right)}^\infty f_X(x)dx\right)f_Y(y)dy, \quad (5)$$

By invoking the respective PDFs and solving inner integral results in

$$Z_0 = \int_U^\infty \sum_{k=0}^{m_{p1}-1}\frac{\left(u_3\left(\psi_2\eta_p\left|\hat{h}_{p,1}\right|^2 + 1\right)\right)^k}{k!}\left(\frac{m_{p1}}{\Omega_{p1}}\right)^k exp^{-\left(\frac{m_{p1}\,u_3\left(\psi_2\eta_p\left|\hat{h}_{p,1}\right|^2+1\right)}{\Omega_{p1}}\right)} f_Y(y)dy \quad (6)$$

By applying the binomial expansion [33, Eq. (1.111)] and solving the involved integral, one can get Eq. (2.15).

Appendix B:

$$P_{out,UE1}^{t_2} = 1 - P_r\left(\frac{\psi_2\,\eta_p|h_{p,1}|^2}{\psi_1\eta_p|h_{p,1}|^2+1} > R_2^{th}\,;\,\frac{\psi_1^{t2}\eta_p|h_{p,1}|^2}{\psi_r\eta_s|h_{s,1}|^2+1} > R_1^{th}\right). \tag{7}$$

Performing some algebraic manipulations on above Eq. (7), one can re-write above equation as

$$\begin{aligned} P_{out,UE}^{t_2} &= 1 - P_r\left(\left|h_{p,1}\right|^2 > u_2\,;\,\left|h_{p,1}\right|^2 > u_6 + u_7\left|h_{p,s}\right|^2\left|h_{s,1}\right|^2\right), \\ &= 1 - P_r\left(|h_{p,1}|^2 > max\left(u_2\,;\,u_6 + u_7|h_{p,s}|^2|h_{s,1}|^2\right)\right), \\ &= 1 - \underbrace{P_r\left(\left|h_{p,1}\right|^2 > u_2\,;\,u_2 > u_6 + u_7\left|h_{s,1}\right|^2\left|h_{p,s}\right|^2\right)}_{Z_2} \\ &\quad - \underbrace{P_r\left(\left|h_{p,1}\right|^2 > u_6 + u_7\left|h_{s,1}\right|^2\left|h_{p,s}\right|^2\,;\,u_2 < u_6 + u_7\left|h_{s,1}\right|^2\left|h_{p,s}\right|^2\right)}_{Z_3}. \end{aligned} \tag{8}$$

where $u_6 = \frac{R_1^{th}}{\psi_1^{t_2}\eta_p}$ and $u_7 = u_6\varphi_r\,\beta\,\eta_p, \bar{U}_0 = \frac{u_2-u_6}{u_7}$.

assuming $\left|h_{p,s}\right|^2 \cong W$ and $\left|h_{s,1}\right|^2 \cong Z$, further Z_2 and Z_3 can be evaluated as

$$Z_2 = \int_{u_2}^{\infty} f_X(x)dx \int_0^{\infty} f_Z(z)F_W\left(\frac{\bar{U}_0}{z}\right)dz, \tag{9}$$

Invoking respective PDFs and CDFs in Eq. (9) and solving the above integral results in Eq.(2.23).

Similarly, Z_3 can be evaluated as follows

$$\left.\begin{aligned} Z_3 &= P_r\left[W < \frac{X-u_6}{u_7\,Z}\,;W \geq \left(\frac{u_7}{Z}\right)\right], \\ &= \int_0^{\infty}\int_{u_6}^{\infty} F_W\left(\frac{X-u_6}{u_7\,Z}\right)f_X(x)\,f_Z(z)dxdz \\ &\quad + \int_0^{u_6} f_X(x)dx - \int_0^{\infty} F_w\left(\frac{u_7}{Z}\right)f_Z(z)dz\,. \end{aligned}\right\} \tag{10}$$

By substituting the corresponding PDFs and CDFs in Eq. (10), and solving the involved integral, one can get the expressions as given Eq. (2.24).

APPENDIX C:

By invoking respective SNRs into Eq. (2.25), and performing some algebraic manipulations on that gives

$$\begin{aligned} P_{out,UE2}^{t2} &= P_r\left(\frac{\psi_2\eta_p\left|h_{p,s}\right|^2}{\psi_1\eta_p\left|h_{p,s}\right|^2+1} > R_2^{th}\ ;\ \frac{\psi_2\eta_s\left|h_{s,\mathbf{2}}\right|^{\mathbf{2}}}{\psi_r\eta_s\left|h_{s,\mathbf{2}}\right|^{\mathbf{2}}+1} < R_2^{th}\right) \\ &+ P_r\left(\frac{\psi_2\eta_p\left|h_{p,s}\right|^2}{\psi_1\eta_p\left|h_{p,s}\right|^2+1} < R_2^{th}\right). \end{aligned} \quad (11)$$

Assuming $\left|h_{s,\mathbf{2}}\right|^{\mathbf{2}} \cong V$ and rearranging above equation can be given as

$$P_{out,UE2}^{t2} = \underbrace{P_r\left(\left|h_{p,s}\right|^2 > u_2\ ;\ \left|h_{s,\mathbf{2}}\right|^{\mathbf{2}} < \frac{u_5}{W}\right)}_{P_1} + \underbrace{P_r\left(\left|h_{p,s}\right|^2 \le u_2\right)}_{P_2}, \quad (12)$$

$$\begin{aligned} P_{out,UE2}^{t2} &= P_1 + P_2\ , \\ &= \int_{u_2}^{\infty} F_w\left(\frac{u_5}{Z}\right) f_W(w)dw + F_W(u_2)\ , \end{aligned} \quad (13)$$

Further $P_{out,UE2}^{t2}$ can be evaluated as follows

$$P_{out,UE2}^{t2} = 1 - \sum_{k=0}^{m_{s2}-1} \frac{\left(\frac{m_{ps}}{\Omega_{ps}}\right)^{m_{ps}}}{\Gamma(m_{ps})k!}\left(\frac{m_{s2}u_5}{\Omega_{s2}}\right)^k \int_{u_2}^{\infty} W^{m_{ps}-k-1} exp^{-\left(\frac{m_{s2}u_5}{\Omega_{s2}W}+\frac{m_{ps}W}{\Omega_{ps}}\right)} dw\ , \quad (14)$$

It is difficult to solve the integral in Eq.(14), hence we use Maclaurin's series to expand term $exp^{-\left(\frac{m_{s2}u_5}{\Omega_{s2}W}\right)}$ as $\sum_{u=0}^{\infty} \frac{(-1)^u\left(\frac{m_{s2}u_5}{\Omega_{s2}}\right)^u}{u!\,W^{-u}}$ and solving the resulting from this expansion, we can derive the expression given by Eq. (2.26)+Eq. (2.27).

Appendix D:

In Eq. (2.31), P_{out2} can be evaluated with the help of Eq. (3.351.1) from [33] and $P_{out,c1}, P_{out,c2}$ can be further evaluated as follows

$$P_{out,c1} = \int_{u_2}^{\infty} F_{X_1}\left(\frac{u_a}{W}\right)\left(1 - \int_{u_2}^{\infty} F_{X_2}\left(\frac{\overline{u}_b}{W}\right)\right) f_W(w)dw \,, \tag{15}$$

By substituting respective PDFs and CDFs in Eq. (15), and integrating the resultant with the help of [34, Eq.(3.351.2)], we can obtain $P_{out,c1}$ as shown in Eq. (2.32).

$$P_{out,c2} = \int_{\phi_1}^{\infty}\left(\int_{\frac{\phi_2}{w}}^{\infty}\left(\int_{0}^{\phi_3 x_2+\frac{u_a}{w}} f_{X_1}(x_1)dx_1 f_{X_2}(x_2)dx_2\right)\right) f_W(w)dw \,, \tag{16}$$

$$= \int_{\phi_1}^{\infty}\left(\int_{\frac{\phi_2}{w}}^{\infty}\left[1 - \sum_{k=0}^{m_{sr}-1} \frac{1}{k!}\left(\frac{m_{sr}}{\Omega_{sr}}\right)^k \left(\phi_3 x_2 + \frac{u_a}{w}\right)^k exp^{-\left(\frac{m_{sr}}{\Omega_{sr}}\left(\phi_3 x_2+\frac{u_a}{w}\right)\right)}\right]\right) f_{X_2}(x_2)dx_2 f_W(w)dw \,, \tag{17}$$

By invoking the associated PDFs then solving the resultant integral with the aid of binomial expansion [33,Eq. (1.111)] and [33,Eq.(3.351.2)], we can get required result for $P_{out,c2}$.

Appendix E:

Transmission rate of Primary user in Type-1:

$$R_1^{pu} = R_{pu}.P_r\left(T_1 log_2(1 + (SNR)_{PU} \geq R_{eq}^{th}\right). \tag{18}$$

Invoking $(SNR)_{PU}$ into above equation leads to

$$R_1^{pu} = R_{pu}.P_r\left(T_1 log_2(1 + \frac{\mu\, \eta_s \left|h_{sj}\right|^2}{(1-\mu)\eta_s \left|h_{sj}\right|^2 + 1}) \geq R_{eq}^{th}\right), \tag{19}$$

$$R_1^p = R_p.P_r\left(\frac{\mu\,\eta_s\,\left|h_{sj}\right|^2}{(1-\mu)\eta_s\,\left|h_{sj}\right|^2+1}) \geq 2^{\frac{R_2^{th}}{T_1}}-1\right), \tag{20}$$

$$R_1^p = R_p.P_r\left(\left|h_{sj}\right|^2 \geq \frac{R_T^{th}}{(\mu-(1-\mu)R_T^{th})\beta\eta_p\left|h_{ps}\right|^2}\right), \tag{21}$$

where $\phi_1 = \frac{R_T^{th}}{((\mu)-(1-\mu)R_T^{th})\beta\eta_p}$, finally the output expression of R_1^{pu} is given as

The final output expression for primary transmission rate is given by

$$R_1^p = R_p\left(1-2\left(\frac{\phi_1\Omega_{ps}}{\Omega_{s1}}\right)^{\frac{1}{2}}K_1\left(2\sqrt{\frac{\phi_1}{\Omega_{s1}\,\Omega_{ps}}}\right)\right). \tag{22}$$

Transmission rate of Secondary user:

$$R_1^{su} = R_{su}.P_r\big(T_1 log_2(1+(SNR)_{SU} \geq\ R_{eq}^{th}\big)\,. \tag{23}$$

Invoking $(SNR)_{SU}$ into above equation leads to

$$R_1^{su} = R_{su}.P_r\left(T_1 log_2(1+\frac{(1-\mu)\,\eta_s\,|h_{sj}|^2}{(\mu)\,\eta_s\,|h_{sj}|^2+1}) \geq\ R_{eq}^{th}\right), \tag{24}$$

$$R_1^{su} = R_{su}.P_r\left(\frac{(1-\mu)\,\eta_s\,\left|h_{sj}\right|^2}{(\mu)\eta_s\,\left|h_{sj}\right|^2+1}) \geq 2^{\frac{R_r^{th}}{T_1}}-1\right), \tag{25}$$

$$R_1^{su} = R_{su}.P_r\left(\left|h_{sj}\right|^2 \geq \frac{R_T^{th}}{((1-\mu)-(\mu)R_T^{th})\beta\eta_p\left|h_{ps}\right|^2}\right), \tag{26}$$

where $\phi_2 = \frac{R_T^{th}}{((1-\mu)-(\mu)R_T^{th})\beta\eta_p}$, finally the output expression of R_1^{su} is given as

$$R_1^{su} = R_{su}\left(1-2\left(\frac{\phi_2\Omega_{ps}}{\Omega_{sr}}\right)^{\frac{1}{2}}K_1\left(2\sqrt{\frac{\phi_1}{\Omega_{sr}\,\Omega_{ps}}}\right)\right). \tag{27}$$

REFERENCES

[1] A. Al-Fuqaha, M. Guizani, M. Mohammadi, M. Aledhari and M. Ayyash, "Internet of Things: A Survey on Enabling Technologies, Protocols, and Applications," in *IEEE Communications Surveys & Tutorials*, vol. 17, no. 4, pp. 2347-2376, Fourthquarter 2015, doi: 10.1109/COMST.2015.2444095.

[2] A. K. Shukla, P. K. Upadhyay, A. Srivastava and J. M. Moualeu, "Enabling Co-Existence of Cognitive Sensor Nodes With Energy Harvesting in Body Area Networks," in *IEEE Sensors Journal*, vol. 21, no. 9, pp. 11213-11223, 1 May1, 2021, doi: 10.1109/JSEN.2021.3062368.

[3] Z. Ding, P. Fan, and H. V. Poor, "Impact of user pairing on 5g nonorthogonal multiple-access downlink transmissions," *IEEE Transactions on Vehicular Technology*, vol. 65, no. 8, pp. 6010–6023, 2016.

[4] Z. Kuang, G. Liu, G. Li and X. Deng, "Energy Efficient Resource Allocation Algorithm in Energy Harvesting-Based D2D Heterogeneous Networks," in *IEEE Internet of Things Journal*, vol. 6, no. 1, pp. 557-567, Feb. 2019, doi: 10.1109/JIOT.2018.2842738.

[5] S. Kumar, U. Dohare, K. Kumar, D. Prasad Dora, K. Naseer Qureshi and R. Kharel, "Cybersecurity Measures for Geocasting in Vehicular Cyber Physical System Environments," in *IEEE Internet of Things Journal*, vol. 6, no. 4, pp. 5916-5926, Aug. 2019, doi: 10.1109/JIOT.2018.2872474.

[6] Z. Ding, P. Fan, and H. V. Poor, "Impact of user pairing on 5g non-orthogonal multiple-access downlink transmissions," *IEEE Transactions on Vehicular Technology*, vol. 65, no. 8, pp. 6010–6023, 2016.

[7] M. R. Palattella *et al.*, "Internet of Things in the 5G Era: Enablers, Architecture, and Business Models," in *IEEE Journal on Selected Areas in Communications*, vol. 34, no. 3, pp. 510-527, March 2016, doi: 10.1109/JSAC.2016.2525418.

[8] S. Haykin, "Cognitive radio: brain-empowered wireless communications," in *IEEE Journal on Selected Areas in Communications*, vol. 23, no. 2, pp. 201-220, Feb. 2005, doi: 10.1109/JSAC.2004.839380.

[9] L. Chen, B. Hu, G. Xu and S. Chen, "Energy-Efficient Power Allocation and Splitting for mmWave Beamspace MIMO-NOMA With SWIPT," in *IEEE Sensors Journal*, vol. 21, no. 14, pp. 16381-16394, 15 July15, 2021, doi: 10.1109/JSEN.2021.3076517.

[10] Y. Saito, A. Benjebbour, Y. Kishiyama, and T. Nakamura, "System-level performance evaluation of downlink non-orthogonal multiple access (NOMA)," in *IEEE 24th Annual International Symposium on Personal, Indoor, and Mobile Radio Communications (PIMRC),* 2013, pp. 611- 615, London, UK.

[11] Y. Liu, Z. Ding, M. Elkashlan, and J. Yuan, "Nonorthogonal multiple access in large-scale underlay cognitive radio networks," *IEEE Trans. Veh. Technol.*, vol. 65, no. 12, pp. 10152-10157, Dec. 2016.

[12] S. Arzykulov, G. Nauryzbayev, T. A. Tsiftsis, B. Maham, and M. Abdallah, "On the outage of underlay CR-NOMA networks with detectand-forward relaying," *IEEE Trans. Cogn. Commun. Netw.*, vol. 5, no. 3, pp. 795-804, Sep. 2019.

[13] L. Lv, Q. Ni, Z. Ding, and J. Chen, "Application of non-orthogonal multiple access in cooperative spectrum-sharing networks over Nakagami-m fading channels," *IEEE Trans. Veh. Technol.,* vol. 66, no. 6 , pp. 5510- 5515, Jun. 2017.

[14] L. Luo, Q. Li, and J Cheng, "Performance analysis of overlay cognitive NOMA systems with imperfect successive interference cancellation," *IEEE Tran. Commun.,* vol. 68, no. 8, pp. 4709-4722, Aug. 2020.

[15] C. K. Singh and P. K. Upadhyay, "Overlay cognitive IoT-based fullduplex relaying NOMA systems with hardware imperfections," *IEEE Internet Things* J., doi: 10.1109/JIOT.2021.3111124.

[16] J. Kim and I. Lee,"Non-Orthogonal multiple access in coordinated direct and relay transmission," *IEEE Commun. Lett.*, vol. 19, no. 11, pp. 2037- 2040, Nov. 2015.

[17] L. Zou, J. Chen, L. Lv, and B. He, “Capacity enhancement of D2D aided coordinated direct and relay transmission using NOMA,” *IEEE Commun. Lett*., vol. 24, no. 10, pp. 2128–2132, Oct. 2020.

[18] Y. Guo, Y. Li, Y. Li, W. Cheng, and H. Zhang, “Swipt assisted noma for coordinated direct and relay transmission,” in 2018 *IEEE/CIC International Conference on Communications* in China (ICCC), 2018, pp. 111–115.

[19] M. Yang, J. Chen, L. Yang, L. Lv, B. He, and B. Liu, “Design and performance analysis of cooperative noma with coordinated direct and relay transmission,” *IEEE Access,* vol. 7, pp. 73 306–73 323, 2019.

[20] Z. Behdad, M. Mahdavi, and N. Razmi, “A new relay policy in RF energy harvesting for IoT networks-A cooperative network approach,” *IEEE Internet Things J*., vol. 5, no. 4, pp. 2715–2728, Aug. 2018.

[21] I. Krikidis, S. Timotheou, S. Nikolaou, G. Zheng, D. W. K. Ng, and R. Schober, “Simultaneous wireless information and power transfer in modern communication systems,” *IEEE Commun. Magazine*, vol. 52, no. 11, pp. 104–110, 2014.

[22] X. Zhou, R. Zhang, and C. K. Ho, “Wireless information and power transfer: Architecture design and rate-energy tradeoff,” *IEEE Trans. Commun.,* vol. 61, no. 11, pp. 4754-4767, Nov. 2013.

[23] A. Rauniyar, P. E. Engelstad, and O. N. Osterbo, “Performance analysis of RF energy harvesting and information transmission based on NOMA with interfering signal for IoT relay systems,” *IEEE Sensors J.,* vol. 19, no. 17, pp. 7668–7682, Sep. 2019.

[24] A. Rauniyar, P. E. Engelstad, and O. N. Østerbø, “On the performance of bidirectional NOMA-SWIPT enabled IoT relay networks,” *IEEE Sensors J.,* vol. 21, no. 2, pp. 2299-2315, 15 Jan., 2021.

[25] Y. Guo, Y. Li, Y. Li, W. Cheng, and H. Zhang, “Swipt assisted noma for coordinated direct and relay transmission,” in IEEE/CIC *International Conference on Communications in China (ICCC),* 2018, pp. 111-115.

[26] X. Yue et al., “Secure communications in a unified non-orthogonal multiple access framework,” *IEEE Trans. Commun.,* vol. 19, no. 3, pp. 2163-2178, Mar. 2020.

[27] Basnayake, Vishaka, Dushantha N.K. Jayakody, Vishal Sharma, Nikhil Sharma, P. Muthuchidambaranathan, and Hakim Mabed. 2020. "A New Green Prospective of Non-orthogonal Multiple Access (NOMA) for 5G" *Information* 11, no. 2: 89. https://doi.org/10.3390/info11020089.

[28] Z. Ding, P. Fan, G. K. Karagiannidis, R. Schober and H. V. Poor, "NOMA Assisted Wireless Caching: Strategies and Performance Analysis," in *IEEE Transactions on Communications*, vol. 66, no. 10, pp. 4854-4876, Oct. 2018, doi: 10.1109/TCOMM.2018.2841929.

[29] J. Yang, C. Ma, J. Man, H. Xu, G. Zheng and H. Song, "Cache-enabled in cooperative cognitive radio networks for transmission performance," in *Tsinghua Science and Technology*, vol. 25, no. 1, pp. 1-11, Feb. 2020, doi: 10.26599/TST.2018.9010137.

[30] J. Yao and N. Ansari, "Caching in Energy Harvesting Aided Internet of Things: A Game-Theoretic Approach," in *IEEE Internet of Things Journal*, vol. 6, no. 2, pp. 3194-3201, April 2019, doi: 10.1109/JIOT.2018.2880483.

[31] Y. Meng, Z. Zhang and Y. Huang, "Cache- and Energy Harvesting-Enabled D2D Cellular Network: Modeling, Analysis and Optimization," in *IEEE Transactions on Green Communications and Networking*, vol.5, no.2, pp. 703-713, June 2021, doi: 10.1109/TGCN.2021.3069506.

[32] S. Gautam, T. X. Vu, S. Chatzinotas and B. Ottersten, "Cache-Aided Simultaneous Wireless Information and Power Transfer (SWIPT) With Relay Selection," in *IEEE Journal on Selected Areas in Communications*, vol. 37, no. 1, pp. 187-201, Jan. 2019, doi: 10.1109/JSAC.2018.2872367.

[33] I. S. Gradshteyn and I. M. Ryzhik, Tables of Integrals, Series and Products, 6th ed. New York: Academic Press, 2000.

[34] A. Nasir, X. Zhou, S. Durrani, and R. Kennedy, “Relaying protocols for wireless energy harvesting and information processing, ” *IEEE Trans. Wireless Commun.,* vol. 12, no. 7, pp. 3622-3636, Jul. 2013.

[35] W. C. Weng and K. Psounis, “Distributed caching and small cell cooperation for fast content delivery,” in Proc. 16th ACM *Int. Symp. Mobile Ad Hoc Networking and Computing,* New York, NY, USA, 2015, pp. 127–136.

[36] K. K. Wong and Z. G. Pan, Array gain and diversity order of multiuser MISO antenna systems, *Int. J. Wireless Inf. Networks,* vol. 15, no. 2, pp. 82–89, 2008.